Permeability prediction in chalks

M. Monzurul Alam, Ida Lykke Fabricius, and Manika Prasad

ABSTRACT

The velocity of elastic waves is the primary datum available for acquiring information about subsurface characteristics such as lithology and porosity. Cheap and quick (spatial coverage, ease of measurement) information of permeability can be achieved, if sonic velocity is used for permeability prediction, so we have investigated the use of velocity data to predict permeability. The compressional velocity from wireline logs and core plugs of the chalk reservoir in the South Arne field, North Sea, has been used for this study. We compared various methods of permeability prediction from velocities. The relationships between permeability and porosity from core data were first examined using Kozeny's equation. The data were analyzed for any correlations to the specific surface of the grain, S_g, and to the hydraulic property defined as the flow zone indicator (FZI). These two methods use two different approaches to enhance permeability prediction from Kozeny's equation. The FZI is based on a concept of a tortuous flow path in a granular bed. The S_g concept considers the pore space that is exposed to fluid flow and models permeability resulting from effective flow parallel to pressure drop. The porosity-permeability relationships were replaced by relationships between velocity of elastic waves and permeability using laboratory data, and the relationships were then applied to well-log data. We found that the permeability prediction in chalk and possibly other sediments with large surface areas could be improved significantly using the effective specific surface as the fluid-flow concept. The FZI unit is appropriate for highly permeable sedimentary rocks such as sandstones and limestones that have small surface areas.

Manuscript received November 2, 2010; provisional acceptance January 6, 2011; revised manuscript received January 24, 2011; final acceptance March 1, 2011.
DOI:10.1306/03011110172

AUTHORS

M. Monzurul Alam ~ *CERE (Center for Energy Resources Engineering), Department of Civil Engineering, Technical University of Denmark, 2800 Kgs. Lyngby, Denmark; mmal@byg.dtu.dk*

M. Monzurul Alam did this work as part of his Ph.D. at the Technical University of Denmark (DTU). He received his master's degree in petroleum engineering from DTU and his B.Sc. degree in mechanical engineering from Rajshahi University of Engineering Technology in Bangladesh. His current focus of research is on rock-fluid interaction and its influence on hydrocarbon reservoir stability.

Ida Lykke Fabricius ~ *CERE (Center for Energy Resources Engineering), Department of Civil Engineering, Technical University of Denmark, 2800 Kgs. Lyngby, Denmark; ilfa@byg.dtu.dk*

Ida Lykke Fabricius is an associate professor at the Technical University of Denmark. Her main responsibility is petrophysics and rock physics of sedimentary rocks. She received her master's degree in geology from Copenhagen University and her Ph.D. and D. Tech. degree from the Technical University of Denmark.

Manika Prasad ~ *Petroleum Engineering Department, Colorado School of Mines, Golden, Colorado; mprasad@mines.edu*

Manika Prasad is an associate professor at Colorado School of Mines. Her main focus is on petrophysics and rock physics of shales and reservoir rocks. She received her diploma in geology and her Ph.D. in geophysics from Kiel University in Germany.

ACKNOWLEDGEMENTS

The financial support from HTF (Danish Advanced Technology Fund) is gratefully acknowledged. We thank DONG Energy for providing well-log and core data. We acknowledge financial support from the Fluids Consortium and the Petroleum Institute, Abu Dhabi.
The AAPG Editor thanks the following reviewers for their work on this paper: John H. Doveton and Colin Stabler.

INTRODUCTION

Permeability describes the movement of fluid in a reservoir. The degree of ease associated with fluid movement in rocks determines the fluid and fluid pressure distribution in a reservoir, and it helps to estimate how much oil can be produced economically. Permeability is an important parameter in three-dimensional reservoir modeling and in assessing the production strategy. Direct in-situ permeability measurements are mostly unavailable, so permeability prediction remains an art instead of a science in petrophysical studies. Models come in numerous flavors from empirical, simple capillary tubes, to neural networks. However, they fail because whereas porosity only depends on the volume of pores, permeability depends on the volumetric and geometric distribution of pores.

Permeability is preferably measured in the laboratory on core plugs. Recovering usable core material by drilling is often costly. Therefore, permeability is frequently predicted from other physical properties of rocks, for example, porosity, seismic velocity, and attenuation. Permeability is classically described as a logarithmic function of porosity. Several authors have reported variation in the porosity-permeability relationship, which mostly depends on sediment composition and diagenesis (Amaefule et al., 1993; Mortensen et al., 1998; Prasad, 2003; Fabricius et al., 2007a). To account for differences in sediment composition, Kozeny (1927) described permeability as a function of porosity and specific surface as a physical measure of pore radius. Biot (1956a, b) theoretically showed that the velocity of elastic waves in rocks depends on both porosity and pore radius as derived from permeability. The findings of Kozeny (1927) and Biot (1956a, b) indicate that permeability should be related to sonic velocity. However, the use of Biot's theory is commonly stymied by lacking information on pore-space parameters.

Velocity-porosity relationships have been extensively studied (Wyllie et al., 1956; Raymer et al., 1980; Nur et al., 1998; Prasad and Dvorkin, 2001; Røgen et al., 2005), whereas velocity-permeability relationships have received less attention. Prasad (2003) showed that velocity-permeability relationships exist in various rocks according to hydraulic reservoir units as defined by the flow zone indicator (FZI), and that FZI may be used in Biot's theory. The concept of the FZI unit is based on modifying Kozeny's (1927) equation so as to improve the porosity-permeability relationships in sandstones (Amaefule et al., 1993). Also based on Kozeny's (1927) equation, Fabricius et al. (2007a) used V_p/V_s ratio and porosity to estimate permeability in carbonate rocks.

Although porosity can be correlated to velocity and to permeability, the relationships are not straightforward. Grain size and shape, sorting, and distributions of secondary minerals (e.g., dolomite) determine the surface area–to–pore volume ratio (specific surface of pores) and thus the difficulty to fluid flow. The presence of fractures can greatly influence the porosity-permeability relationship on a reservoir scale; indeed, the magnitude of fracture permeability in chalk reservoirs (e.g., Valhall field, North Sea) may be in the range of 1000 to 10,000 md, whereas fracture porosity has an insignificant contribution to total porosity (Rogers et al., 2007). However, in this article, we limit our scope to matrix properties. The size and distribution of grains in a carbonate rock can cause a distinction between pore-body size and pore-throat size to be relevant (Pourmohammadi et al., 2007). In this case, permeability is defined by the pore-throat size, not the pore size, and permeability could be significantly low even if the porosity is high. However, North Sea chalks are primarily mudstones and wackestones according to the Dunham (1962) classification, where pore connectivity is high and pore size is fairly uniform (Røgen et al., 2005). From nuclear magnetic resonance transverse relaxation time (T_2) relaxation, Alam et al. (2010a) found that free-flowing fluid does not exist in chalk. Therefore, we did not consider the effects of pore throats in these sediment types.

Sedimentary rocks undergo diagenetic processes after burial. Mechanical compaction causes porosity reduction: velocity may increase because of increased grain contact and permeability decreases as porosity decreases. Recrystallization by contrast makes the grains smoother, in principle, without change in porosity: permeability increases because of a smaller specific surface, but the effect on velocity is only minor, unless recrystallization

causes cementation at the grain contacts. Contact cementation thus increases velocity, whereas porosity is unaffected. Pore-filling cementation (lithification) causes porosity to decrease and velocity to increase significantly (Dvorkin and Nur, 1996; Du Bernard et al., 2003), whereas specific surface with respect to pore space becomes larger (Borre and Fabricius, 1998) and permeability decreases. Therefore, the relationship between velocity and permeability should take these geologic and geometric factors into consideration.

The diagenetic processes that any given chalk went through can be identified by changes in the specific surface (Borre and Fabricius, 1998). The specific surface may be expressed relative to total volume or relative to pore space or relative to grain volume. Previous studies of chalk indicate that the specific surface of the grain, S_g, tends to be closer to a constant for a given stratigraphic unit than the specific surface of pores or of total volume (Fabricius et al., 2007a). As changes in specific surface affect both permeability and sonic velocity, we examined the variation of permeability with compressional velocity of sound waves in chalk while referring to S_g. We also examined the applicability of the FZI method in chalk that Prasad (2003) had successfully applied in sandstones and limestones. Velocity-permeability and velocity-porosity relationships from the core plug data were checked in terms of S_g units and FZI units. The established relationships between velocity and permeability as derived from core data according to S_g units and FZI units were then used to predict permeability directly from velocity. For comparison, permeability was also predicted from porosity, calculated from the velocity-porosity relationship for each S_g unit and FZI unit. Each method was tested for permeability prediction using well-log compressional wave velocity data. We were specifically interested in understanding the controls on permeability in the chalks with a high–specific surface area as opposed to the sandstones and limestones with a low specific surface area.

North Sea Chalk

Calcareous sediments cover about 48% of the world's sea floor (Sverdrup et al., 1942), and 60% of the world's oil lies in carbonate reservoirs (Akbar et al., 2000). A significant amount of hydrocarbons in the North Sea is placed in chalk reservoirs. The low permeability of this chalk is a great challenge for hydrocarbon production. More efficient production strategies could be designed by having a better means of mapping its permeability.

Chalk is a sedimentary rock, developed from the diagenesis of pelagic calcareous ooze. Particles in calcareous ooze are primarily the skeletons of algae called coccospheres. The spherical coccospheres are between 10 and 30 μm in diameter and composed of 7 to 20 wheel-shaped coccolith platelets that are 2- to 20-μm in diameter and 0.5 to 2.5 μm across (Scholle, 1977; D'Heur, 1984). However, North Sea chalk is predominantly composed of coccolith fragments or aggregates of coccolith platelets; entire coccospheres are relatively rare (Scholle, 1977). This makes chalk a very fine grained homogeneous rock with a high specific surface area. A high S_g also means that the fluid is exposed to a large surface. Therefore, more force is required to move this fluid to overcome friction, leading to very low permeabilities (a fraction of a millidarcy to a few millidarcys) in chalk.

Despite low permeabilities, North Sea chalks may have high porosities (as much as 50%). Newly deposited oceanic calcareous ooze has porosity between 70 and 80%. Porosity reduces to 60% during the first hundred meters of burial, mostly caused by mechanical compaction (Schlanger and Douglas, 1974; Hamilton, 1976; Scholle, 1977). Soon after deposition, the recrystallization process starts and smoothens the calcite crystals and allows further compaction and porosity reduction until grain contact cement starts to form (Borre and Fabricius, 1998; Fabricius, 2003). Fabricius (2003) proposed that grain-contact cement is most likely to form at a low compaction rate, whereas a high compaction rate allows further mechanical compaction. Below a burial depth of about 1 km (0.6 mi), in fully drained oceanic settings, pore-filling cementation reduces porosity to 10 to 20%. North Sea hydrocarbon reservoirs may be situated at more than 2 km (>1.2 mi) depth. The porosity of chalk at this depth should be about 15% under normal circumstances (Scholle, 1977). Overpressure causing

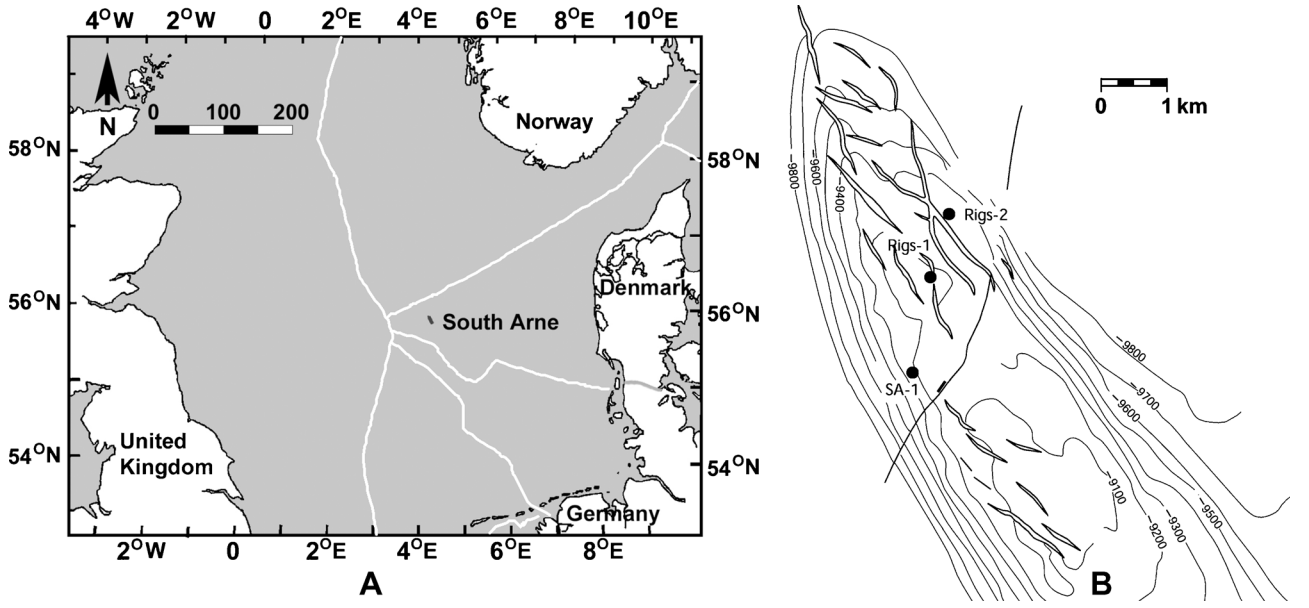

Figure 1. (A) The location map of South Arne field, North Sea. (B) The position of the studied wells within the field, plotted on top of the chalk group depth structure map (modified from Larsen, 1998). Depth indicates true vertical depth subsea (TVDSS) in feet.

low normalized or "effective" burial depth (Japsen, 1998) and also incursion of hydrocarbons before significant pore-filling cementation are possible porosity-preserving mechanisms in North Sea chalk (Scholle, 1977; D'Heur, 1984; Andersen, 1995).

The Ekofisk Formation of the Paleocene and the Tor Formation of the Late Cretaceous from the South Arne field, Danish North Sea, were investigated (Figure 1), as these are hydrocarbon reservoirs. These two formations are mostly calcitic but have different silica and clay contents. In general, the Ekofisk Formation rocks have a high specific surface area because of their high content (>12%) of silica and clay (Røgen and Fabricius, 2002). The smaller specific surface area in the Tor Formation rocks is caused by low (<5%) contents of silica and clay (Fabricius et al., 2008). Typical specific surface areas for the various constituents of a typical North Sea chalk are given in Table 1. The specific surface of chalk containing clay and silica mostly depends on the contribution from these phases. Therefore, by accounting for the specific surface area, we can indirectly evaluate lithology variations.

Because of the variation in the specific surface with chalk composition, porosity-permeability relationships vary significantly stratigraphically. As a rule for a given porosity, the permeability of the Ekofisk Formation is lower than the permeability of the Tor Formation (Andersen, 1995). The variation in permeability of chalk can be addressed by dividing the formations into units according to the S_g. An equivalent strategy is to assign a series of different FZIs.

Porosity-Permeability Relationship

Despite having a high porosity, chalk can have a low matrix permeability. Several authors (Scholle,

Table 1. Typical Specific Surface of the Minerals in North Sea Chalk

Mineral	Specific Surface (m^2/g)	Reference
Calcite	2*	Madsen and Lind, 1998
	0.5–3.5*	Røgen and Fabricius, 2002
	App. 5*	Røgen and Fabricius, 2002
Quartz	0.7*	Madsen and Lind, 1998
	10*	Madsen and Lind, 1998
Kaolinite	15*	Røgen and Fabricius, 2002
	5–40	Britannica Online, 2010
	60*	Røgen and Fabricius, 2002
Smectite	40–800	Britannica Online, 2010

*North Sea data.

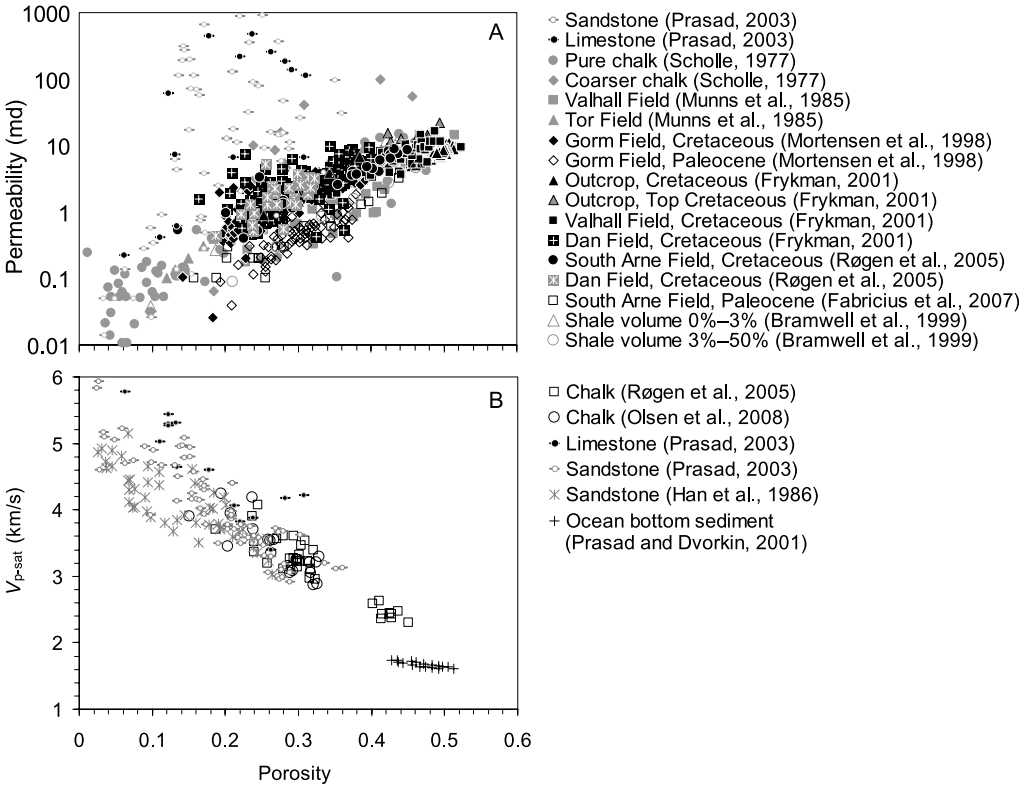

Figure 2. (A) The porosity-permeability trends for chalk published in literature. Dark closed and dark open data points are chalk from the Tor Formation and Ekofisk Formation of the North Sea, respectively. Gray closed points represent North Sea chalk from unknown formations. Limestone and sandstone (samples of Prasad, 2003) are indicated, respectively, by gray and black dashes with a circle in the middle. The trends for North Sea chalk can be primarily divided into two segments. Sandstone and limestone as studied by Prasad (2003) have significantly higher permeability for a given porosity than North Sea chalk. (B) The relationship between porosity and compressional wave velocity ($V_{p\text{-}sat}$) as measured in brine-saturated North Sea chalk and a few other sedimentary rocks.

1977; Munns, 1985; Klimentos and McCann, 1990; Mortensen et al., 1998; Bramwell et al., 1999; Frykman, 2001; Røgen et al., 2005; Fabricius et al., 2007b) have published porosity-permeability data for North Sea chalk (Figure 2). For porosities more than 20%, the permeability of chalk may be several orders of magnitude lower than that in sandstones (Figure 2A). Chalk with a high carbonate content (pure chalk) and a porosity more than 20% has about 1 md permeability. The permeability of impure chalk (>10% noncarbonate fraction) is sometimes below the detection limit (typically 0.01 md) of a conventional gas permeameter. Published data presented in Figure 2A show that despite having similar porosities, North Sea chalk permeabilities vary by as much as three orders of magnitude. This variation can be explained by differences in contents of clay and silica, as expressed in the specific surface (Røgen and Fabricius, 2002). Therefore, the variation in the porosity-permeability relationship in North Sea chalk is highly influenced by the noncarbonate fraction that determines the S_g.

Mortensen et al. (1998) found that air permeability in chalk is independent of the type of porosity (e.g., intraparticle, interparticle), and they suggested a porosity-permeability relationship, avoiding the tortuosity concept by introducing a porosity dependent "*c*" factor, $c(\phi)$ in the Kozeny's equation. The physical meaning of $c(\phi)$ is described in the theory section.

Porosity-Velocity Relationship

Porosity is considered to be the major controlling factor of the velocity of the elastic wave in rocks (Figure 2B). In clay-free homogeneous chalk, at a given stage of diagenesis, velocity may be inversely correlated with porosity. In analogy to the work on

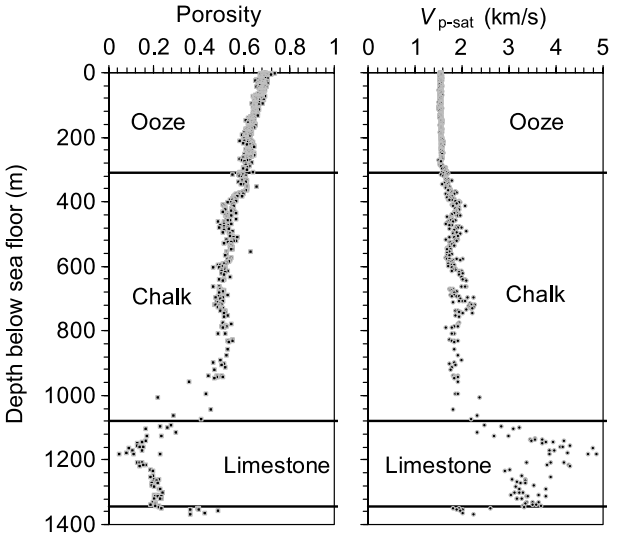

Figure 3. The porosity and compressional wave velocity ($V_{p\text{-}sat}$) versus vertical depth below sea floor (mbsf) show the change in porosity and sonic velocity during diagenesis: An example from Ocean Drilling Program (ODP) leg 130, site 807, core data from the ODP database (Kroenke et al., 1991). Both porosity and velocity trends depend on the type of sediment or sedimentary rock.

sandstones (Han et al., 1986), it is plausible that only a few volume fractions of clay could change such a trend significantly (Han et al., 1986). Røgen et al. (2005) found that the porosity-velocity relationship in chalk also depends on the type of clay minerals. For the same porosity, samples with kaolinite have higher velocities than samples with smectite. Based on data from Ocean Drilling Program Leg 130, site 807, Fabricius (2003) showed that the porosity-velocity trend changes during the diagenetic process (Figure 3). Compressional wave velocity remains almost constant until the ooze starts to transform into chalk. Velocity increases with depth in the chalk interval, indicating the growth of grain contact cement. Limestone develops as a result of pore-filling cementation. The decrease in porosity and increase of velocity over a short depth interval occurs at the transition between chalk and limestone (Figure 3). Thus, we see that the velocity-porosity relationship is made complicated by the geometric distribution of pores and cements.

In this article, we will compare permeability predicted from velocity with the more conventional indirect process involving porosity predictions from velocity and then the use of sonic porosity to estimate permeability. Because both velocity and permeability are governed by volumetric and geometric considerations, whereas porosity is only a volumetric description, the factors controlling the porosity-velocity relationship could also govern the porosity-permeability relationship. Therefore, by statistical analysis of the data, we will assign an FZI, and for comparison, an S_g to intervals of the reservoir.

THEORY

Tortuosity and Flow in Porous Media

It is widely defined in literature that fluid flow in porous media occurs in a tortuous path (Kozeny, 1927; Carman, 1937; Amaefule et al., 1993), where the length of actual equivalent channel for fluid flow is longer than the physical length of a porous medium (Figure 4A). On the more simple assumption that a granular bed is analogous to a group of capillaries parallel to the direction of flow, Darcy (1856) developed a fluid-flow equation through porous media:

$$Q = k\frac{A}{\mu}\frac{\Delta P}{l} \qquad (1)$$

where k is permeability, ΔP is the pressure difference over length, l, with cross sectional area A, and μ is the dynamic viscosity of the flowing fluid.

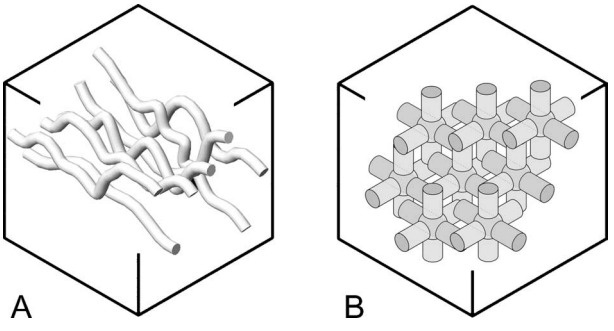

Figure 4. The conceptual flow through a porous rock. All porosities are shown in gray shade. (A) The flow in a tortuous path. The actual equivalent flow length (l_e) is longer than the net traveled distance because of the curved flow path. (B) The concept of flow path in pore space with a high connectivity (adapted from the concept of Mortensen et al., 1998). Branches with dark gray shades are aligned in the direction of flow.

Darcy's equation is based on Poiseuille's law for the flow of a viscous fluid through a capillary tube:

$$Q = \frac{\pi d_e^4}{128\mu}\frac{\Delta P}{l} \tag{2}$$

where d_e is the equivalent diameter of the capillary tube.

Flow Zone Indicator

Based on laminar flow of fluid in porous media, Kozeny (1927) derived

$$k = c\frac{\phi^3}{S^2} \tag{3}$$

$$k = c\frac{1}{S_g^2}\frac{\phi^3}{(1-\phi)^2} \tag{4}$$

where k is liquid permeability (Klinkenberg, 1941), ϕ is porosity, and c is Kozeny's constant. Kozeny (1927) found that the value of c is about 0.25. Entities S and S_g are grain surface per unit bulk volume and grain surface per volume of grains, respectively. Carman (1937) presented Kozeny's equation as

$$k = \frac{1}{F_s\tau^2 S_g^2}\frac{\phi^3}{(1-\phi)^2} \tag{5}$$

where F_s is a dimensionless shape factor and τ is tortuosity defined as the ratio between a conceptual actual flow length, l_a, and sample length, l ($\tau = l_a/l$) (Figure 4A). It can be seen that $1/F_s\tau^2$ replaces Kozeny's constant. It varies with the internal structure of the sediments and thus also with specific surface but may be assumed as fairly constant within the same hydraulic unit (Amaefule et al., 1993). Rearranging equation 5, Amaefule et al. (1993) addressed the variability of Kozeny's constant as follows:

$$\left[\sqrt{\frac{k}{\phi}}\right]\left[\frac{\phi}{(1-\phi)}\right]\left[\frac{1}{\sqrt{F_s}\tau S_g}\right] \tag{6}$$

$$[RQI] = [\varepsilon][FZI] \tag{7}$$

$$\log RQI = \log\varepsilon + \log FZI \tag{8}$$

where RQI is the reservoir quality index, ε is the void ratio, and FZI is described as the flow zone indicator:

$$\mathrm{FZI} = \frac{1}{\sqrt{F_s}\tau S_g} = \frac{1}{\varepsilon}\sqrt{\frac{k}{\phi}} \tag{9}$$

When permeability and FZI are expressed in millidarcys and micrometers, respectively, we obtain

$$\mathrm{FZI} = \frac{0.0314}{\varepsilon}\sqrt{\frac{k}{\phi}} \tag{10}$$

Because the FZI describes geometric distributions of pores and grains, Prasad (2003) used this approach to describe the variations in velocity-porosity relations. The geometric control of pore-volume distribution was found to also describe velocity variations with permeability (Prasad, 2003).

Specific Surface of the Grains

The surface area of minerals is widely estimated by the BET nitrogen adsorption technique introduced by Brunauer, Emmett, and Teller (Brunauer et al., 1938). In this method, surface area, S_{BET}, per unit weight is estimated by allowing nitrogen gas to adsorb on the surface of the rock. Knowing the grain density, ρ_g, of the minerals, the S_g is calculated

$$S_g = S_{BET} \times \rho_g \tag{11}$$

The specific surface with respect to the bulk, S, and specific surface with respect to pore, S_ϕ, is calculated as (Borre and Fabricius, 1998)

$$S = (1-\phi)S_g \tag{12}$$

$$S_\phi = \frac{S}{\phi} \tag{13}$$

Effective Specific Surface

For homogeneous fine-grained sediments like chalk, pores are likely to have high connectivities, so the

concept of a torturous flow path is difficult to perceive. In such rocks, in addition to the capillaries parallel to the direction of flow (as defined by Darcy, 1856), there should be capillaries in the directions perpendicular to the flow (Figure 4B). Although the resultant flow occurs only in one direction, fluid flows in all capillaries. A major loss of pressure (according to Poiseuille's law) occurs in the direction of the resultant flow. In the direction normal to the direction of pressure drop, fluid flow may be seen as practically an instantaneous pressure transfer (Røgen and Fabricius, 2002). This perception could be compared with the process of climbing a hill, where work required for the movement parallel to the horizon is negligible compared with the work required for vertical movement.

Mortensen et al. (1998) used this concept by projecting the pore space into the form of orthogonal interpenetrating tubes. Rocks with high connectivities in pore space could be imagined as a system of such tubes (Figure 4B). A part of the porosity in such a system is thus insignificant in the resultant flow because of shielding by solids. Mortensen et al. (1998) quantified the porosity that is active to the flow in a given direction, where Poiseuille's law is valid by introducing a porosity-dependent $c(\phi)$ (to distinguish from Kozeny's constant c in equation 3):

$$c(\phi) = \left[4\cos\left\{\frac{1}{3}\text{arc}\cos(2\phi - 1) + \frac{4}{3}\pi\right\} + \right]^{-1} \quad (14)$$

Theoretically, the value of c is 1 when all the pores are aligned as parallel tubes in the direction of flow and is 0 when aligned as perpendicular tubes to the flow. This porosity-dependent $c(\phi)$ replaces the term c of Kozeny's equation (equation 5). Entity $c(\phi)$ increases with increasing porosity as visualized by the volume of perpendicular interpenetrating tubes in Figure 4B. The point is that this volume increases as porosity increases. Decreasing $c(\phi)$ results in a higher shielding effect and will have the same effect in the equation as a conceptual tortuous path with a higher actual equivalent travel length (l_e). The advantage of using the concept of $c(\phi)$ is that it can be predicted directly from ϕ and does not affect the specific surface term. With porosity-dependent c, Kozeny's equation becomes

$$k = c(\phi)\frac{\phi^3}{S^2} \quad (15)$$

Using the relation stated in equation 12,

$$k = c(\phi)\frac{1}{S_{g-eff}^2}\frac{\phi^3}{(1-\phi)^2} \quad (16)$$

where S_{g-eff} is the effective specific surface, which in chalk is similar to or only slightly lower than the S_g measured by the BET nitrogen adsorption technique (Mortensen et al., 1998). A high homogeneity at particle scale is probably the reason why chalk permeability in this way may be predicted directly from Kozeny's equation without fitting factors. We calculated S_{g-eff} from equation 16 using core permeability and porosity measured in the laboratory:

$$S_{g-eff} = \sqrt{c(\phi)\times\phi}\frac{\phi}{(1-\phi)}\sqrt{\frac{1}{k}} \quad (17)$$

The S_{g-eff} does not depend on the porosity because it is not a property of the bulk rock but a property of the particles that make up the rock. For homogeneous rocks, the variation of effective porosity for flow, due to varying porosity is determined by $c(\phi)$. Therefore, for a given porosity, permeability variation can be resolved by the difference of specific surface alone.

DATA SET

We used 31, 1.5-in. and 12, 1-in. core samples from SA-1 and Rigs-1 wells of South Arne field in central North Sea (Table 2). The carbonate content of each sample was measured by treating the finely powdered sample with an excess of 0.5 mol/L hydrochloric acid and subsequent titration with 0.5 mol/L sodium hydroxide. The specific surface

Table 2. Physical Properties of the Tested Samples from Rigs-1 (RE and RT) and SA-1 (SE and ST)

Sample ID	Formation	TVDSS* (m)	ϕ (%)	Grain Density (g/cm^3)	Carbonate Content (%)	k_g (md)	Specific Surface (m^2/g)	$V_{p\text{-dry}}$ (km/s)	$V_{s\text{-dry}}$ (km/s)	$V_{p\text{-sat}}$ (km/s)	$V_{s\text{-sat}}$ (km/s)
RE-06A	Ekofisk	2762.2	32.1	2.70	75.9	0.5	3.9	3.63	2.16	3.06	1.83
RE-08B	Ekofisk	2762.2	31.9	2.70	75.9	0.5	3.9	3.51	2.07	3.62	2.17
RE-09B	Ekofisk	2762.3	30.0	2.69	79.0	0.5	3.6	3.55	2.09	3.63	2.18
RE-10A	Ekofisk	2762.3	30.7	2.70	79.0	0.5	3.6	3.76	2.26	3.34	1.80
RE-12B	Ekofisk	2762.3	29.9	2.69	79.0	0.5	3.6	3.85	2.29	3.42	1.84
RE-14A	Ekofisk	2765.1	31.1	2.70	77.9	0.5	3.7	–	–	3.63	2.18
RE-22A	Ekofisk	2771.3	32.9	2.71	88.2	1.1	3.8	3.20	1.95	3.17	1.60
RE-23A	Ekofisk	2771.4	32.0	2.72	88.3	0.6	3.5	3.29	1.97	3.28	1.62
RE-24	Ekofisk	2771.5	35.9	2.72	88.3	0.9	3.6	2.81	2.16	2.86	2.19
RE-26B1	Ekofisk	2774.3	30.9	2.71	89.7	0.5	2.9	–	–	3.20	1.67
RE-26B2	Ekofisk	2774.3	29.5	2.71	89.7	0.5	2.9	–	–	3.30	2.10
RE-28A1	Ekofisk	2774.3	28.9	2.70	89.7	0.8	2.9	–	–	3.63	2.18
RE-29	Ekofisk	2774.5	28.0	2.71	89.0	0.4	3.2	3.62	2.29	3.33	1.74
RE-31	Ekofisk	2774.5	29.1	2.71	89.0	0.6	3.2	–	–	3.29	2.02
RE-C2E-A	Ekofisk	2765.3	18.3	2.72	84.8	0.1	3.6	–	–	–	–
RE-C2E-B	Ekofisk	2765.3	17.7	2.71	84.8	0.1	3.6	–	–	–	–
RT-01	Tor	2798.7	38.9	2.71	95.2	4.4	2.1	2.70	1.68	2.81	1.65
RT-02	Tor	2798.8	35.0	2.72	95.2	2.3	2.1	3.37	2.02	3.40	1.70
RT-03	Tor	2802.5	42.3	2.71	96.7	4.8	1.9	1.98	1.26	2.43	1.48
RT-C3G-A	Tor	2802.7	42.5	2.74	96.7	5.6	2.0	–	–	–	–
SE-02	Ekofisk	2791.6	16.3	2.71	77.5	0.02	6.4	2.99	1.99	3.39	1.54
SE-03	Ekofisk	2791.6	17.6	2.71	77.5	0.04	6.4	2.71	1.89	3.32	1.77
SE-05A	Ekofisk	2783.6	26.2	2.72	81.2	0.1	5.2	2.81	2.07	3.01	1.79
SE-C1B7-A	Ekofisk	2783.7	26.1	2.71	77.5	0.1	5.2	–	–	–	–
ST-03B	Tor	2849.6	29.2	2.71	99.1	1.7	1.7	3.18	2.08	–	–
ST-04B	Tor	2862.2	27.8	2.71	99.0	1.3	1.6	3.76	2.20	–	–
ST-07	Tor	2855.6	31.3	2.72	99.9	2.7	1.6	3.13	1.92	–	–
ST-08A	Tor	2855.6	32.3	2.71	99.9	3.2	1.7	3.03	2.05	–	–
ST-08B	Tor	2855.5	31.0	2.71	99.9	2.6	1.6	2.81	1.86	–	–
ST-13B	Tor	2843.0	30.8	2.71	99.5	2.2	1.9	3.11	1.94	–	–
ST-16B	Tor	2837.0	28.5	2.72	99.0	1.2	1.8	3.46	2.11	–	–
ST-23A	Tor	2825.1	26.2	2.72	98.6	0.8	1.7	3.90	2.14	3.82	1.90
ST-24A	Tor	2825.1	26.3	2.72	98.2	0.8	1.7	3.68	2.23	3.67	1.97
ST-24B	Tor	2825.1	24.8	2.72	98.2	0.8	1.7	4.11	2.42	4.12	2.20
ST-26	Tor	2825.0	28.2	2.71	98.5	1.1	1.6	3.57	2.13	–	–
ST-C5B11-C	Tor	2830.9	28.4	2.72	97.8	0.6	2.1	–	–	–	–
ST–C5B20-D	Tor	2837.0	27.6	2.73	99.3	1.1	1.8	–	–	–	–
ST-C5B2-C	Tor	2825.1	29.1	2.72	98.6	0.8	2.3	–	–	–	–
ST-C6B12-F	Tor	2849.6	31.2	2.73	99.1	2.0	1.7	–	–	–	–
ST-C6B2-C	Tor	2843.1	29.9	2.73	99.5	1.6	1.8	–	–	–	–
ST-C7B14-C	Tor	2862.2	29.6	2.73	99.0	1.9	1.6	–	–	–	–
ST-C7B4-A	Tor	2855.6	26.1	2.74	98.9	3.7	1.4	–	–	–	–
ST-C7B4-I	Tor	2855.6	32.7	2.74	98.9	3.6	1.4	–	–	–	–

*TVDSS = true vertical depth subsea.

of each sample was estimated by the BET nitrogen adsorption technique (Brunauer et al., 1938). Grain density, ρ_g, and porosity, ϕ, were obtained from helium porosimetry. Qualitative information of mineralogy was obtained by the x-ray diffraction method.

Gas permeability, k_g, was measured by nitrogen injection. Equivalent liquid (Klinkenberg corrected) permeability, k, was calculated using the relationship for North Sea chalk presented by Mortensen et al. (1998):

$$k = 0.52 \times k_g^{1.083} \tag{18}$$

where k and k_g are given in millidarcys.

Compressional wave velocity, V_p, and shear wave velocity, V_s, were measured by recording the traveltime of transmitted ultrasonic waves at 132 kHz through a sample of known length. Measurements were taken while the sample was placed between the two pistons of a loading frame and applying 4 MPa axial stress and 1.33 MPa radial stress, which simulate the effective stress geometry at reservoir conditions. Reservoir rocks are subjected to both vertical and lateral stresses as well as high pore pressure (overpressure) in the North Sea chalk reservoirs. To simulate reservoir stress in a laboratory experiment requires only the application of the differential stress (total stress minus pore pressure) instead of the actual stresses (Teeuw, 1971). The effective vertical stress in South Arne field is between 10 and 20 MPa (1450–2901 psi), but because velocity variation in North Sea chalk samples was found to be less than 3% between 4 and 11 MPa (580–1595 psi) (Borre and Fabricius, 2001), we used 4 MPa (580 psi) for our sample to avoid damage in the sample.

As a reference, 44 core data from Fabricius et al. (2008) were also used; they include data from wells Rigs-1, Rigs-2, and SA-1. Compressional wave velocity data from wireline logs of SA-1 and Rigs-1 were used for permeability prediction. The predicted permeability was compared with core permeability from the Geological Survey of Denmark and Greenland (GEUS) core laboratory database. All core data sets include porosity and permeability, as well as V_p and V_s under both water-saturated and dry conditions.

RESULTS

Mineralogy of the Studied Interval

The samples from Ekofisk Formation contain as much as 25% noncarbonate fraction (Table 2). The distribution of noncarbonates is recognizable in backscattered electron images at large magnification, and some of the pores are thus partially filled with clay (Figures 5, 6, indicated by arrows). Fabricius et al. (2008) showed that varying amounts of quartz could reside as submicrometer-size crystal aggregates loosely arranged with clay in interparticle porosity. Such allocation of the carbonate and noncarbonate phase will increase the surface: pore volume ratio and make fluid flow difficult in the kaolinite-rich Rigs-1 well. The Ekofisk Formation in SA-1 is rich in smectite and almost impermeable (Table 2). The Ekofisk Formation also contains considerable amounts of preserved large hollow microfossils, which would tend to reduce the surface: pore volume ratio, but the effect of this does not make up for the effect of clay. The Tor Formation, however, contains a homogeneous matrix of calcareous nannofossil debris (Figure 6).

Selection of Method

In practice, effective S_g and FZI work the same way and only use a different approach in describing the difficulty of flow in porous media. The difference in the approach using S_g and FZI may be expressed as follows: In the S_g unit approach, the Kozeny *c-factor* is seen as a function of porosity only, whereas in the FZI unit approach, the Kozeny *c-factor* is expressed in terms of specific surface. Therefore, effective S_g and FZI differ roughly by a multiplier in a log-log scale plot (Figure 7A). However, the relationship between S_g calculated from the BET nitrogen adsorption technique (Brunauer et al., 1938) and S_{g-eff} is scattered around a linear trend on a log-log plot (Figure 7C). A minor part

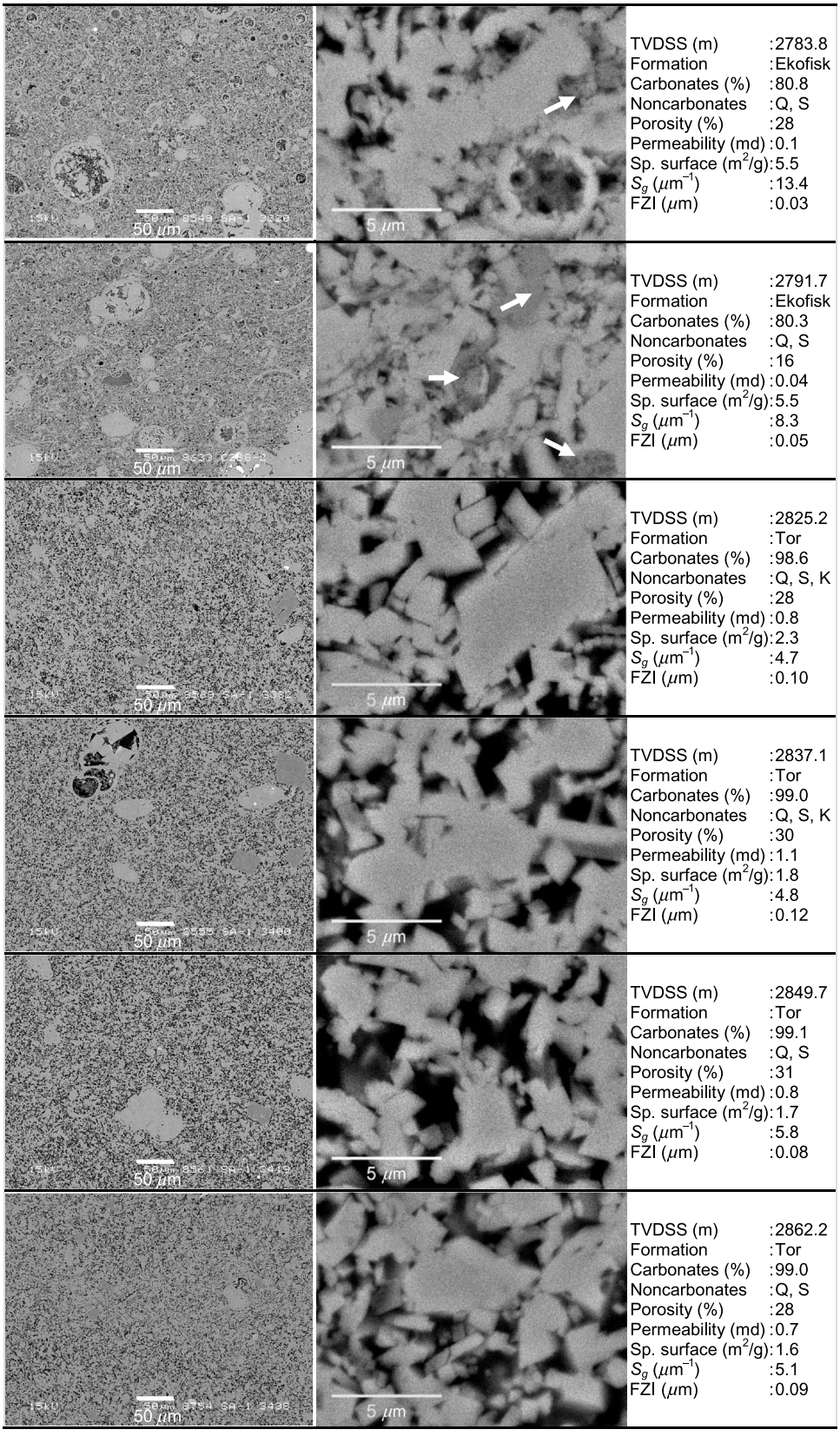

Figure 5. Backscatter electron (BSE) micrographs of epoxy-impregnated and polished samples from well SA-1 at two magnifications, plotted according to true vertical depth subsea (TVDSS) in meters. Dark is porosity and bright is calcite. Clay and quartz appear as gray (indicated by arrows). The top two are Ekofisk Formation samples, and the bottom four are Tor Formation samples. The letters Q, S, and K represent quartz, smectite, and kaolinite, respectively. The specific surface of the grains (S_g) is calculated from the bulk specific surface measured by the BET (Brunauer, Emmett, and Teller) nitrogen adsorption technique (Brunauer et al., 1938) and grain density (equation 11). The flow zone indicator (FZI) is calculated from porosity and measured liquid permeability (equation 10).

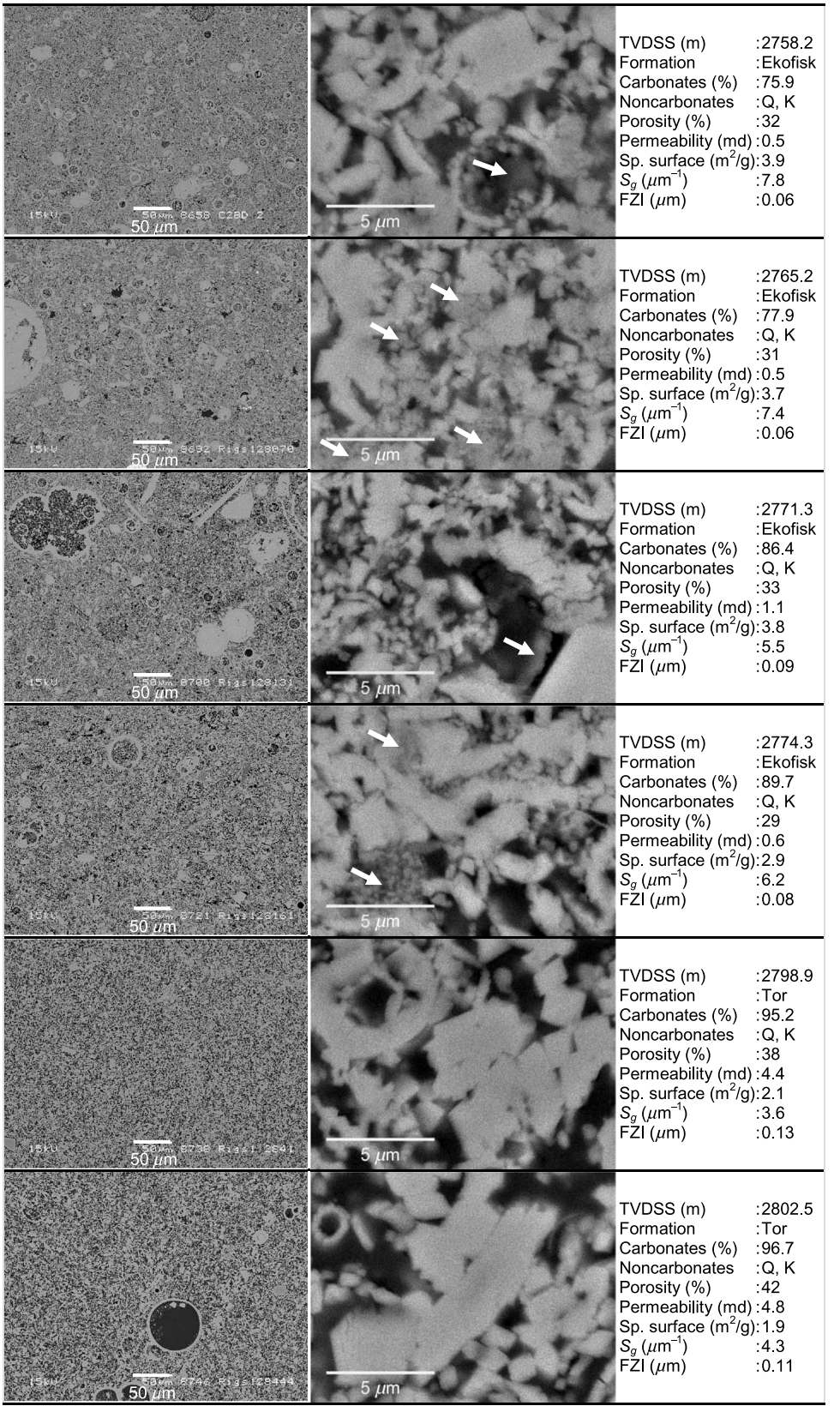

Figure 6. Backscatter electron (BSE) micrographs of epoxy-impregnated and polished samples from well Rigs-1 at two magnifications, plotted according to true vertical depth subsea (TVDSS) in meters. Dark is porosity, and bright is calcite. Clay and quartz appear as gray (indicated by arrows). The top four are Ekofisk Formation samples, and the bottom two are Tor Formation samples. The letters Q and K represent quartz and kaolinite, respectively. The specific surface of the grains (S_g) is calculated from bulk specific surface measured by the BET (Brunauer, Emmett, and Teller) nitrogen adsorption technique (Brunauer et al., 1938) and grain density (equation 11). The flow zone indicator (FZI) is calculated from porosity and measured liquid permeability (equation 10).

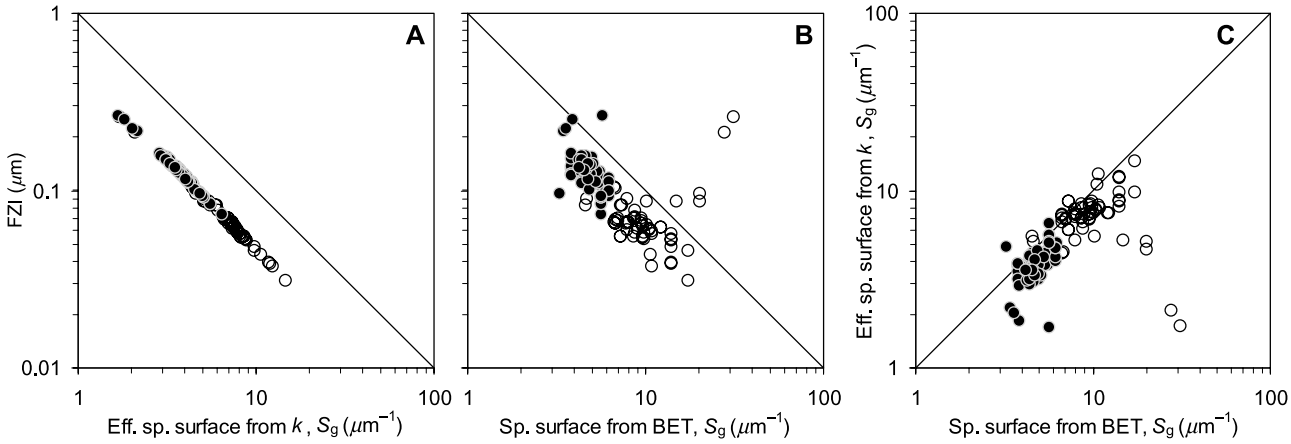

Figure 7. The relationship of flow zone indicator (FZI) with (A) effective specific surface of the grains (S_{g-eff}) calculated from equation 17 using Klinkenberg permeability and (B) specific surface of the grains (S_g) calculated from the bulk specific surface measured by the BET (Brunauer, Emmett, and Teller) nitrogen adsorption technique (Brunauer et al., 1938) and grain density (equation 11). (C) Calculated S_{g-eff} versus measured S_g specific surface. Open symbols indicate Ekofisk Formation, and closed symbols indicate Tor Formation.

of the difference may arise from the crushing of samples before BET measurement, but the difference between S_g and S_{g-eff} in the studied samples is larger than in Gorm field (Mortensen et al., 1998), so the difference may well be caused by a still small but not insignificant heterogeneity on the pore scale of the South Arne samples. The S_{g-eff} calculated from porosity and permeability may tend to be low because gas permeability is measured at ambient conditions or at pressures lower than reservoir pressures. Thus, some fractures that would normally be closed at reservoir conditions may remain open in the laboratory (Hamilton, 1976). In this case, the permeability measured from gas injection should be higher than the matrix permeability and thus cause relatively low S_{g-eff}. However, the permeability calculated from the specific surface could give lower than actual permeability (Figure 8), as the BET method estimates all the surface area exposed to nitrogen gas and Kozeny's equation assumes sample homogeneity. However, some of this surface may not be active in flow according to Poiseuille's law, but be the relevant interface for description of sonic wave transmission.

In our velocity-permeability study, we used S_g calculated from BET. As the modeling by effective S_g and FZI are so similar in practice, we chose for comparison to use the FZI concept in the velocity-permeability study to be able to compare with literature data (Prasad, 2003).

Flow Zone Indicator Unit and Specific Surface of the Grain Unit Separation

The porosity-permeability relationship shows a notable separation of samples from the Ekofisk and Tor formations (Figure 9). From the distribution of

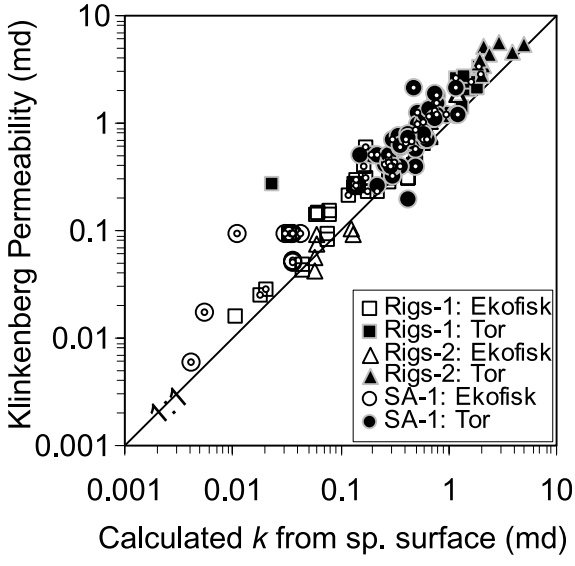

Figure 8. The relationship between Klinkenberg permeability calculated from air permeability (Mortensen et al., 1998) and permeability calculated from specific surface measured by the BET (Brunauer, Emmett, and Teller) nitrogen adsorption technique (Brunauer et al., 1938) by using the modified Kozeny's equation (equation 15). Open symbols represent Ekofisk Formation, and closed symbols represent Tor Formation. Data points with a circle inside indicate the present data set.

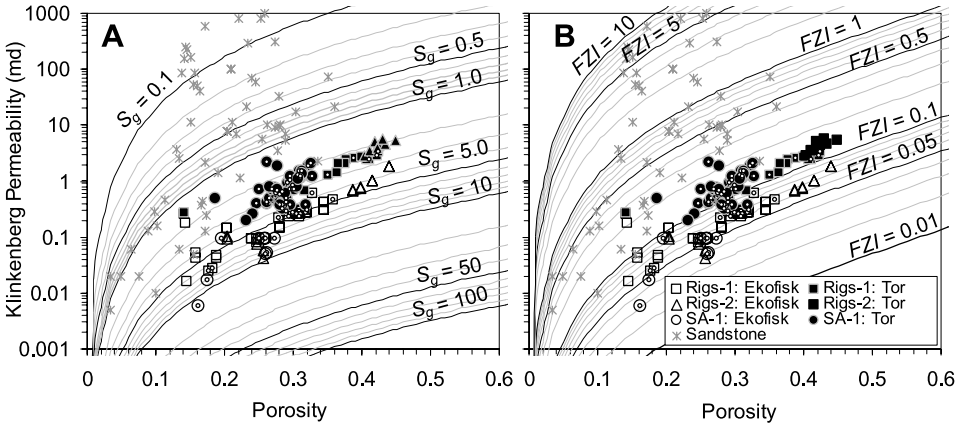

Figure 9. Theoretical and experimental relationships between porosity and permeability according to the (A) specific surface of the grains (S_g) units and (B) flow zone indicator (FZI) units. The curves of (A) were calculated from equation 15 using $c(\phi)$ values from equation 14. The curves of (B) were calculated from equation 10. Data points with a circle inside indicate the present data set.

permeability, we could define three S_g units in the Ekofisk Formation and one S_g unit in the Tor Formation (Figure 10). Similarly, two FZI units in the Ekofisk Formation and two FZI units in the Tor Formation were also assigned.

Our data show that from the variation of S_g and FZI with depth, we could separate distinct units that coincided with stratigraphic units (Figure 11). Not all S_g units and FZI units are present in every well. The studied wells are situated several kilometers apart (Figure 1B).This indicates stratigraphic variation in the distribution of minerals and spatial variation in deposition or preservation of units. With respect to S_g, both Tor and Ekoisk formations vary among the wells (Figures 5, 6). The Rigs-1 well contains mostly kaolinite clay; whereas SA-1 contains smectite clay, which has a much higher specific surface than kaolinite (Madsen and Lind, 1998). Although the studied formations in the SA-1 well are deeper than in Rigs-1, they are located in the same stratigraphic unit. Therefore, we expect that the variation in noncarbonate content is caused by the spatial position of the wells instead of stratigraphy.

The S_g units do not show significant variation in the Tor Formation (Figure 10). According to the FZI units, one additional stratigraphic unit (TFZI2) could be defined at the bottom of the Tor Formation (Figure 11F). In Rigs-1 and Rigs-2, two S_g units in the Ekofisk Formation (ESG2 and

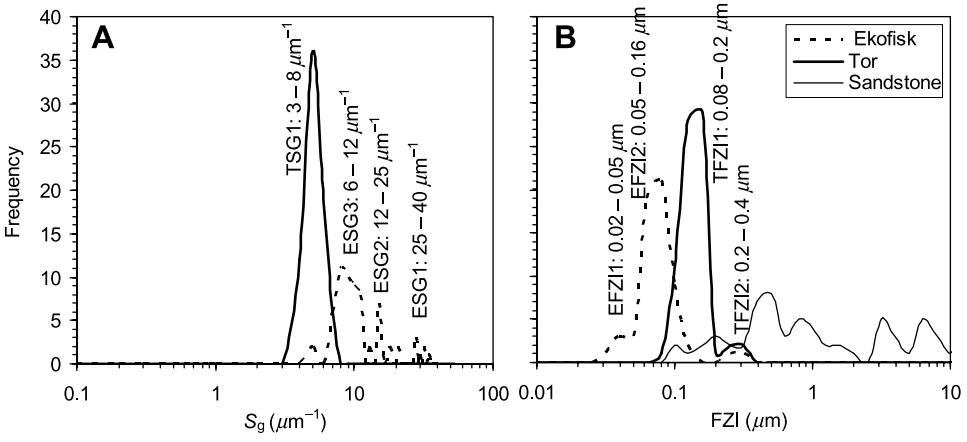

Figure 10. The distribution of samples according to the (A) specific surface of the grains (S_g) units and (B) flow zone indicator (FZI) units. The S_g units and FZI units are assigned when there is a peak in distribution, as indicated on the plots. To get a reasonable trend, S_g units and FZI units were only assigned where numbers of samples are three or more. The distribution of FZI for sandstone (thin continuous line), calculated by using Prasad's (2003) porosity and permeability data, indicates a significant difference from FZI distribution of chalk. ESG = Ekofisk Formation S_g unit; TSG = Tor Formation S_g unit; EFZI = Ekofisk Formation FZI unit; TFZI = Tor Formation FZI unit.

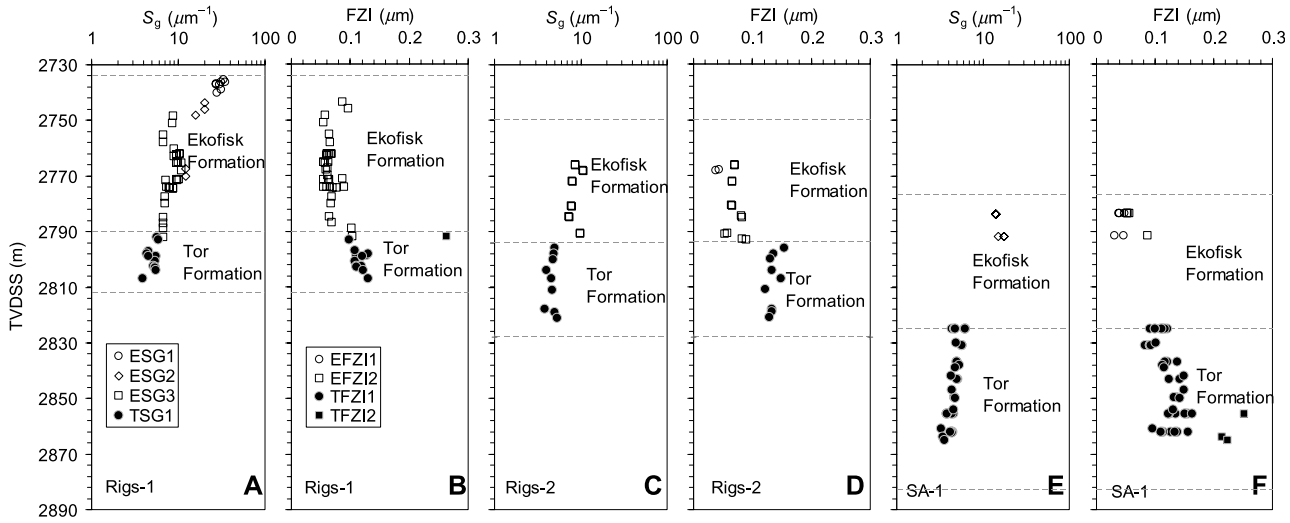

Figure 11. The specific surface of the grains (S_g) units and flow zone indicator (FZI) units in the wells Rigs-1, Rigs-2 and SA-1. In a plot of true vertical depth subsea (TVDSS), S_g units and FZI units indicate a distinct stratigraphic unit. ESG = Ekofisk Formation S_g unit; TSG = Tor Formation S_g unit; EFZI = Ekofisk Formation FZI unit; TFZI = Tor Formation FZI unit.

ESG3) exist, whereas SA-1 is only represented by ESG1.

Velocity-Permeability Relationship in Assigned Specific Surface of the Grain Unit and Flow Zone Indicator Unit

We examined the relationship between compressional wave velocity and permeability (both measured in core plugs in the laboratory) according to the assigned S_g units and FZI units for samples in both dry and saturated conditions (Figure 12). Within the assigned S_g units and FZI units, significant correlations were found where a large number of samples (ESG3, TSG1, EFZI2, and TFZI1) exist; the correlation coefficients for velocity-permeability correlations were 0.7 or better. In ESG1, ESG2, EFZI1, and TFZI2, no significant correlation could be achieved because of a low number of samples. These samples may represent local variation of mineralogy.

The velocity-permeability relationships established here were then applied to the same set of velocity data to calculate permeability for the respective S_g units and FZI units. Predicted permeability was then compared with the Klinkenberg permeability. Furthermore, these relationships were applied to log-measured compressional wave velocity data and compared with the GEUS database permeability.

Velocity-Porosity Relationship in Assigned Specific Surface of the Grain Unit and Flow Zone Indicator Unit

In a more traditional procedure, V_p-porosity relationships were established according to the designated S_g units and FZI units (Figure 13). The porosity calculated from these relationships was used for permeability calculation. Predicted permeability was then compared with the Klinkenberg permeability. The same relationships were applied to log-measured compressional wave velocity data to compare the predicted permeability with GEUS database permeability.

The predicted permeability according to S_g units and FZI units is close to the measured permeability when permeability is predicted directly from V_p according to S_g units and FZI units (Figure 14). The variation between measured and predicted permeability is higher when predicted indirectly via porosity from velocity and then permeability from porosity (Figure 15). In the indirect method, the predicted permeability could be underestimated by more than 35% in the Tor Formation when the S_g method is applied as specific surface measured by the BET method is higher. The FZI method works satisfactorily in this case. However, for the low-permeability and impure Ekofisk Formation, permeability is overestimated when the indirect

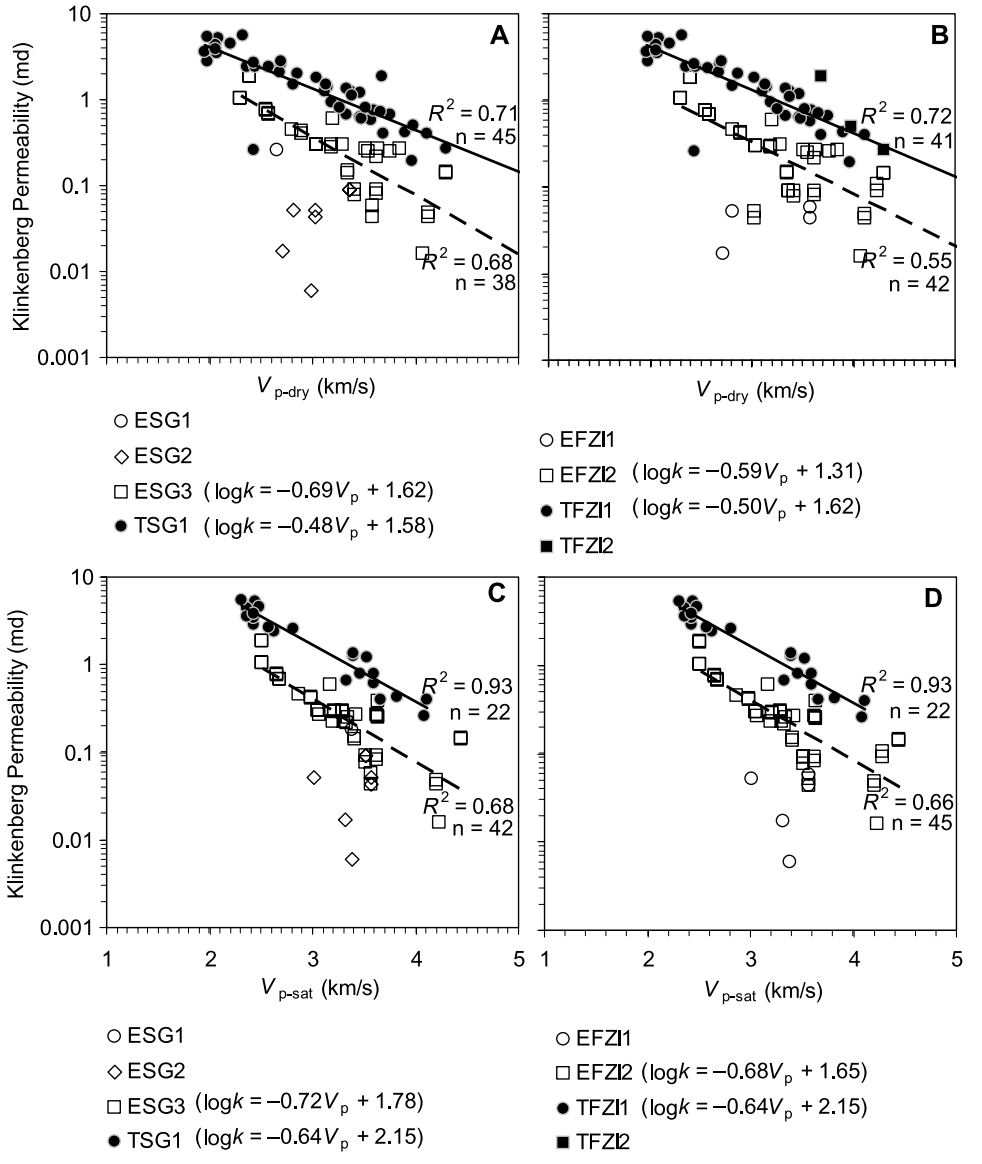

Figure 12. Compressional wave velocity (V_p)–Klinkenberg permeability (k) relationships according to the designated specific surface of the grains (S_g) units (A, C) and flow zone indicator (FZI) units (B, D); A and B for dry data ($V_{p\text{-}dry}$), and C and D for saturated data ($V_{p\text{-}sat}$). Solid data points are the Tor Formation, and open data points are the Ekofisk Formation. Ekofisk Formation trends are indicated by broken lines, and Tor Formation trends are indicated by continuous lines. ESG = Ekofisk Formation S_g unit; TSG = Tor Formation S_g unit; EFZI = Ekofisk Formation FZI unit; TFZI = Tor Formation FZI unit.

method is used in the FZI method. By knowing the specific surface of the Ekofisk Formation, permeability prediction could be improved marginally, although scatters more than ±35% of the measured permeability.

DISCUSSION

Permeability Prediction from Velocity

In general, permeability and velocity have a negative correlation (Figure 12). However, the slope of the relationship defines a specific S_g unit or FZI unit. Permeability decreases faster as velocity increases in chalk with a higher specific surface and a lower FZI (ESG3, EFZI2) compared with the chalk with lower S_g because of low clay and silicate contents (TSG1, TFZI1).

At very high porosity, the assigned S_g units become close to each other and FZI units show a similar trend. This indicates that at high porosity, velocity is less influenced by the impurities in chalks or by permeability itself. With the decrease in porosity, a general trend is that velocity increases faster in cleaner chalk (lower S_g and higher FZI) than chalks containing clay and quartz (higher specific surface and higher FZI) (Figure 13).

Sound wave propagation in chalk primarily depends on the contact between chalk grains, whereas

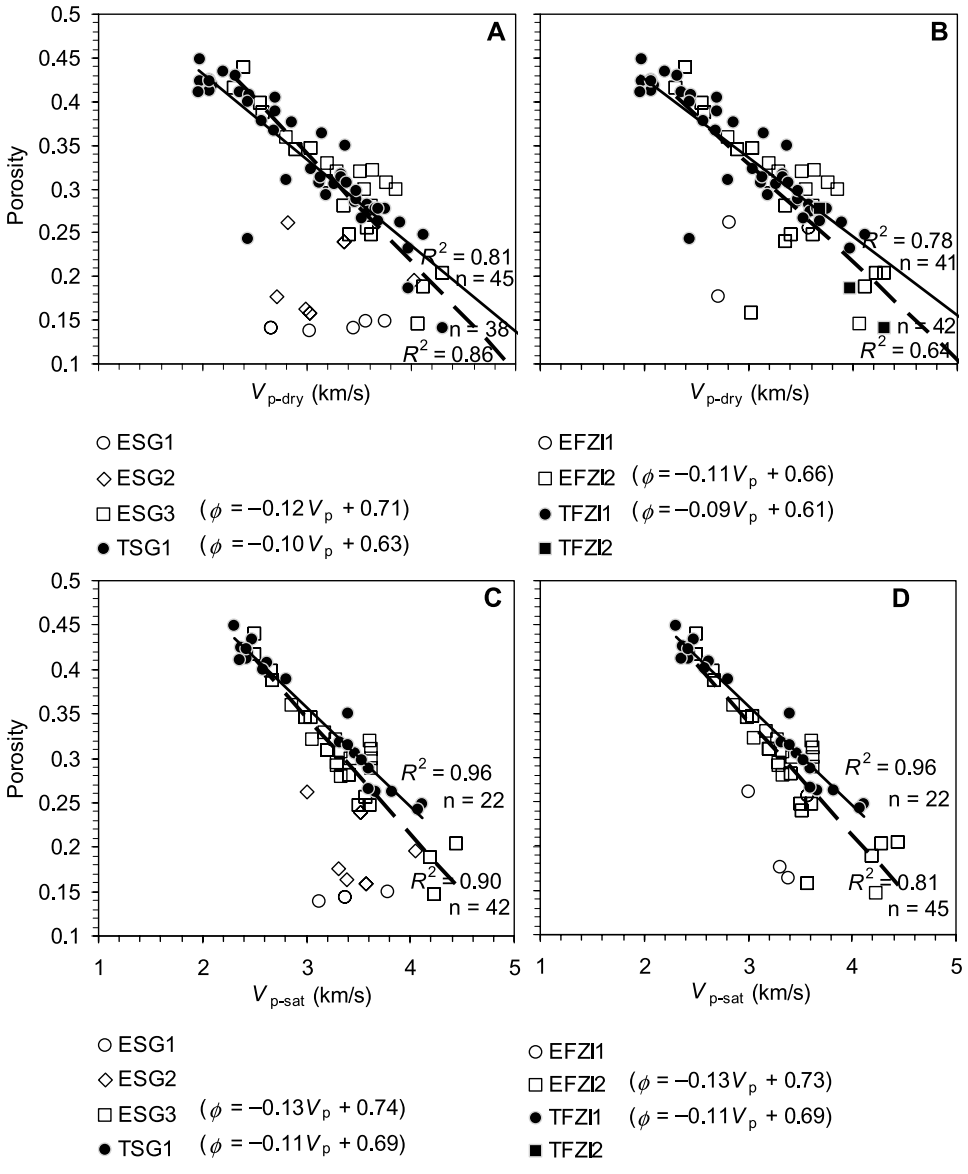

Figure 13. Compressional wave velocity (V_p)–porosity (ϕ) relationships according to the designated specific surface of the grains (S_g) units and flow zone indicator (FZI) units. Panels A and B are for dry data ($V_{p\text{-}dry}$), and C and D are for saturated data ($V_{p\text{-}sat}$). Solid data points are Tor Formation, and open data points are Ekofisk Formation. Ekofisk Formation trends are indicated by broken lines, and Tor Formation trends are indicated by continuous lines. ESG = Ekofisk Formation S_g unit; TSG = Tor Formation S_g unit; EFZI = Ekofisk Formation FZI unit; TFZI = Tor Formation FZI unit.

permeability in chalk mostly depends on dispersed clay and silicate grains (Figures 5, 6) inside the pore space because they provide most of the flow-hindering surfaces (Table 1). These suspended particles have comparatively less influence on the stiffness (and velocity) of chalk (Fabricius, 2003). At lower porosity, some of these silicates can act as a frame and increase stiffness and thus velocity of elastic waves. For the same porosity, a cemented pure calcite frame is stiffer than a frame made of several minerals because of poor or no contact cement. Therefore, velocity is higher in a pure calcite frame compared with a combined mineral frame.

During the diagenetic process of chalk, major porosity reduction occurs because of compaction (Fabricius, 2001; Alam et al., 2010b). During compaction, calcite grains come close to each other, pushing the suspended noncarbonates into the pore space. Thus, the ratio of noncarbonate volume to pore volume increases. This process decreases the permeability substantially. Therefore, permeability reduction is much faster in impure chalk compared with velocity increase from the same amount of porosity reduction.

In a $V_{p\text{-}sat}$-porosity plot, the assigned S_g units and FZI units may be easily detected, whereas it is difficult to distinguish the assigned S_g units and FZI units in a $V_{p\text{-}dry}$-porosity plot (Figure 13). This could be caused by specific surface–dependent influence of water (water softening) (Fabricius et al., 2010).

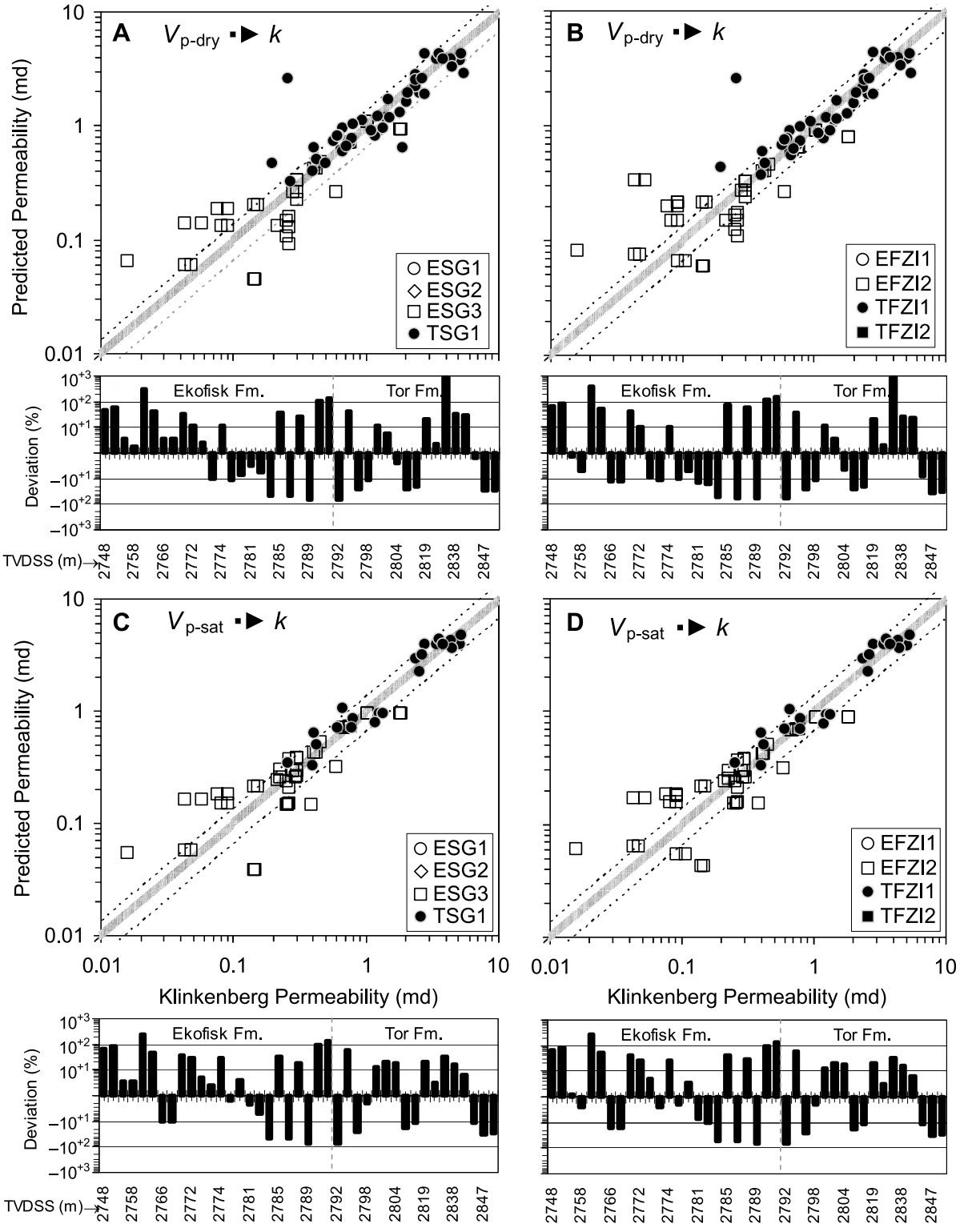

Figure 14. The predicted permeability directly from velocity versus measured Klinkenberg permeability (k) according to (A, C) the designated specific surface of the grains (S_g) units and (B, D) flow zone indicator (FZI) units. Panels A and B are using compressional wave velocity ($V_{p\text{-}dry}$) measured in dry samples, and C and D are using compressional wave velocity ($V_{p\text{-}sat}$) measured in saturated samples. The shaded area indicates 5% standard deviation, and the area between the two dotted lines indicates 35% standard deviation. Deviation (in percentage) from the measured permeability in the laboratory for different stratigraphic units is given below each figure in a plot of deviation versus true vertical depth subsea (TVDSS). ESG = Ekofisk Formation S_g unit; TSG = Tor Formation S_g unit; EFZI = Ekofisk Formation FZI unit; TFZI = Tor Formation FZI unit.

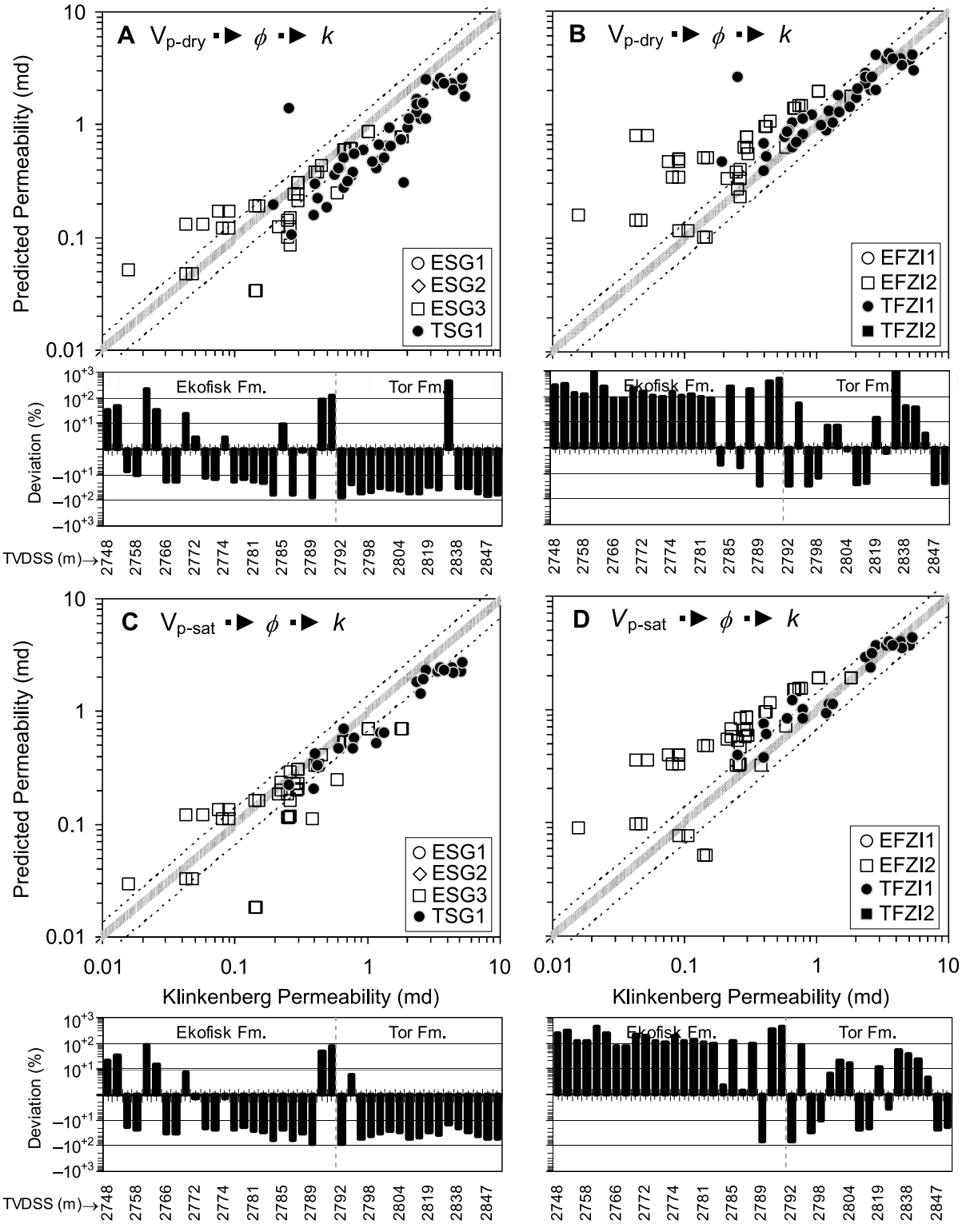

Figure 15. The predicted permeability from porosity (ϕ), where porosity was calculated from velocity data plotted against measured Klinkenberg permeability according to the designated specific surface of the grains (S_g) units (A, C) and flow zone indicator (FZI) units (B, D). Panels A and B are using compressional wave velocity ($V_{p\text{-}dry}$) measured in dry sample, and C and D are using compressional wave velocity ($V_{p\text{-}sat}$) measured in saturated samples. The shaded area indicates 5% standard deviation, and the area between two dotted lines indicate 35% standard deviation. Deviation (in percentage) from the measured permeability in the laboratory for different stratigraphic units is given below each figure in a plot of deviation versus true vertical depth subsea (TVDSS). ESG = Ekofisk Formation S_g unit; TSG = Tor Formation S_g unit; EFZI = Ekofisk Formation FZI unit; TFZI = Tor Formation FZI unit.

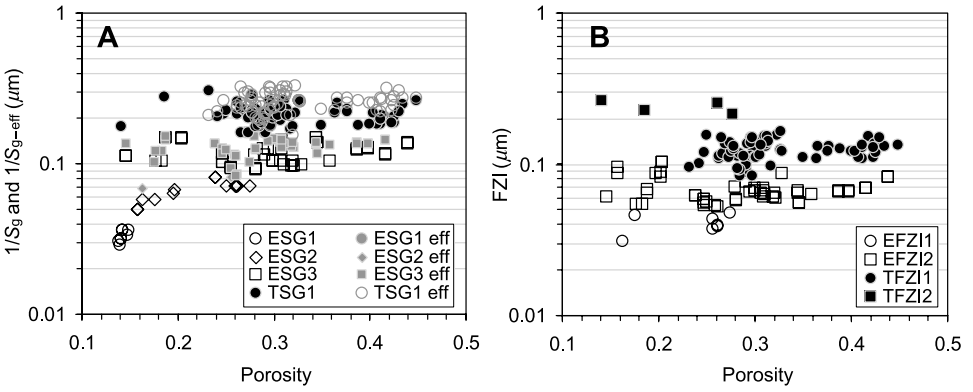

Figure 16. (A) The relationship of porosity with the effective specific surface of the grains ($S_{g–eff}$) calculated from equation 17 using measured liquid permeability and specific surface of the grains (S_g) calculated from bulk specific surface measured by the BET (Brunauer, Emmett, and Teller) nitrogen adsorption technique (Brunauer et al., 1938) and grain density (equation 11). Gray data points indicate $S_{g–eff}$, and black data points indicate S_g. (B) Relationship between porosity and flow zone indicator (FZI) units. ESG = Ekofisk Formation S_g unit; TSG = Tor Formation S_g unit; EFZI = Ekofisk Formation FZI unit; TFZI = Tor Formation FZI unit.

The prediction of permeability from porosity alone is only possible with a high degree of uncertainty. Permeability in chalk is highly influenced by its content of noncarbonates. By using S_g unit separation, we may consider the noncarbonate fraction in chalk because it constitutes a significant part of the specific surface. However, FZI units separate rocks with different degrees of tortuosity into different hydraulic flow units. It is possible to define a relevant S_g unit or FZI unit for a particular formation from the porosity-core permeability plot. Comparison of Figure 12 with Figure 13 shows that in the velocity-permeability plot, separation is marginally better using S_g units as compared with using FZI units. Permeability can be closely predicted from the previously assigned velocity-permeability relationship for that particular specific surface (Figures 14, 15). The use of dry velocity data or saturated velocity data does not make a significant difference in permeability prediction for cores.

Predicted Permeability by Specific Surface of the Grain Unit and Flow Zone Indicator Unit Separation

A plot of porosity versus S_g measured by the BET method (Brunauer et al., 1938) and $S_{g–eff}$ calculated from permeability (equation 17) does not show a significant variation with porosity for $S_{g–eff}$ (Figure 16).

Table 3. Statistical Analysis of Permeability Prediction

	MSE*		MAE**		$R^{\dagger}$	
Method	Ekofisk Formation	Tor Formation	Ekofisk Formation	Tor Formation	Ekofisk Formation	Tor Formation
$V_{p\text{-}sat}\rightarrow k$, S_g	0.07	0.3	0.12	0.43	0.87	0.89
$V_{p\text{-}sat}\rightarrow k$, FZI	0.08	0.3	0.13	0.43	0.87	0.89
$V_{p\text{-}dry}\rightarrow k$, S_g	0.07	0.7	0.11	0.59	0.86	0.82
$V_{p\text{-}dry}\rightarrow k$, FZI	0.09	0.7	0.15	0.59	0.85	0.82
$V_{p\text{-}sat}\rightarrow\phi\rightarrow k$, S_g	0.12	2.0	0.18	1.1	0.87	0.89
$V_{p\text{-}sat}\rightarrow\phi\rightarrow k$, FZI	0.23	0.4	0.39	0.5	0.86	0.89
$V_{p\text{-}dry}\rightarrow\phi\rightarrow k$, S_g	0.10	2.3	0.15	1.2	0.86	0.83
$V_{p\text{-}dry}\rightarrow\phi\rightarrow k$, FZI	0.22	0.8	0.39	0.6	0.85	0.81

*MSE = calculated mean standard error.
**MAE = mean absolute error.
†R = correlation coefficient.

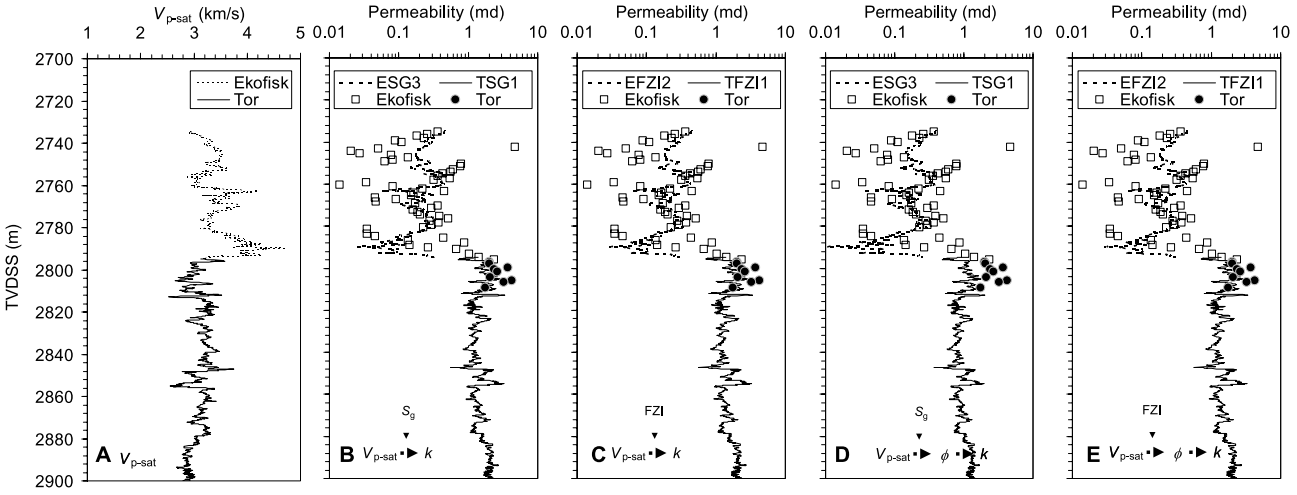

Figure 17. The predicted permeability for Rigs-1 logging data. (A) Compressional wave velocity at saturated condition ($V_{p\text{-}sat}$). (B, C) The permeability estimated directly from $V_{p\text{-}sat}$ for the assigned specific surface of the grains (S_g) units and flow zone indicator (FZI) units, respectively. (D, E) The permeability predicted from porosity (calculated from $V_{p\text{-}sat}$) for the assigned (S_g) units and (FZI) units, respectively. TVDSS = true vertical depth subsea (in meters). ESG = Ekofisk Formation S_g unit; TSG = Tor Formation S_g unit; EFZI = Ekofisk Formation FZI unit; TFZI = Tor Formation FZI unit.

By using porosity-dependent $c(\phi)$ in equation 17, $S_{g\text{–eff}}$ becomes independent of porosity for a particular S_g unit. Thus, in the velocity-permeability relationship, $S_{g\text{–eff}}$ remains the only dependent factor. It enables us to predict permeability from velocity, if $S_{g\text{–eff}}$ is known.

We observed that samples with a high noncarbonate content show a low FZI value (low connectivity) (Figures 5, 6). By assigning an FZI value for a particular lithology, the permeability-velocity and porosity-velocity relationships could be narrowed. Thus, a better prediction of permeability was achieved (Figures 14, 15). However, for less than 1 md permeability, predicted permeability varies significantly from the calculated permeability. It indicates the difficulty of defining a hydraulic unit by means of the FZI unit separation in low-permeability chalk. Variations between the predicted

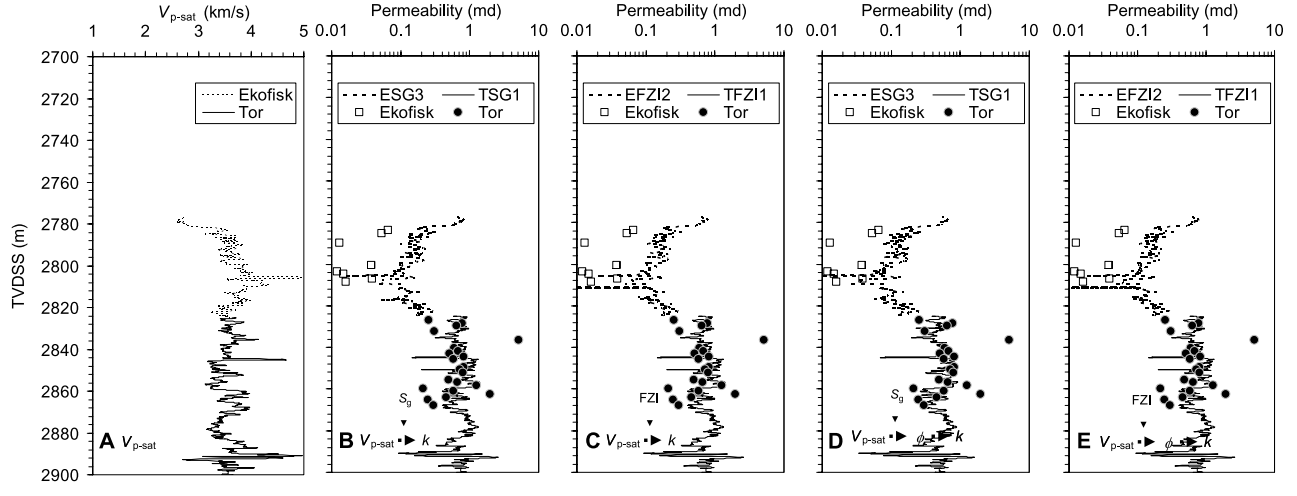

Figure 18. The predicted permeability for SA-1 logging data. (A) Compressional wave velocity ($V_{p\text{-}sat}$) at saturated condition. (B, C) The permeability estimated directly from $V_{p\text{-}sat}$ for the assigned specific surface of the grains (S_g) units and flow zone indicator (FZI) units, respectively. (D, E) The permeability predicted from porosity (calculated from $V_{p\text{-}sat}$) for the assigned (S_g) units and (FZI) units, respectively. TVDSS = true vertical depth subsea (in meters). ESG = Ekofisk Formation S_g unit; TSG = Tor Formation S_g unit; EFZI = Ekofisk Formation FZI unit; TFZI = Tor Formation FZI unit.

permeability from the calculated permeability could be reduced by assigning more FZI units in low-permeability chalk. However, it requires more core data and makes it difficult to apply in well logs.

The calculated mean standard error (MSE), mean absolute error (MAE), and correlation coefficient (R) between predicted and measured permeability are presented in Table 3. Although the error in prediction in the SA-1 Tor Formation by the S_g method is higher than that in the FZI method, both methods show a high correlation coefficient (≥0.8), which validates the applicability of the methods for permeability prediction. However, the S_g method has one advantage in that it is applicable without knowing the permeability: it requires specific surface that is measured from the side trims and end trims or cuttings, and therefore, no core plug is required.

Implication to Well-Log Velocity

We applied relationships established between velocity and permeability and velocity and porosity to predict the permeability for wells Rigs-1 (Figure 17) and SA-1 (Figure 18). We used $V_{p\text{-}sat}$ data achieved from wireline logging. The predicted permeability was compared with the laboratory permeability database. Because Tor Formation chalk is less affected by mineralogical variation, its permeability can be predicted very closely to the core permeability by considering its S_g between 2 and 7 μm^{-1} (TSG1) and FZI value between 0.08 and 0.2 μm (TFZI1). However, in the low-permeability Ekofisk Formation, permeability could only be predicted within one order of magnitude of the core-measured permeability. Core data of Rigs-1 and SA-1 indicate that the S_{g-eff} of Ekofisk Formation is between 7 and 10 μm^{-1} (ESG2) and FZI value between 0.04 and 0.2 μm (EFZI2).

CONCLUSIONS

For low-permeability (<10 md) sedimentary rocks such as North Sea chalk, permeability variation for the same porosity rock could be described well by separating into units of S_g or into FZI. Separating units according to effective specific surface S_{g-eff} is in practical terms equivalent to using FZI. Grouping samples according to S_g units and FZI units improves the permeability prediction from compressional velocity. The S_g unit or FZI unit splitting according to lithology enables us to predict permeability within less than a single order of magnitude, whereas the general porosity-permeability relationship varies three orders of magnitude in chalk. If specific surface of a particular chalk unit is known, the velocity-permeability relationship for that unit can be applied to predict permeability directly from the compressional wave velocity. The S_g unit splitting could be applied effectively to predict the permeability of low-permeability chalk. The FZI unit separation may give better results for high-permeability (>10 md) sedimentary rocks.

REFERENCES CITED

Akbar, M., et al., 2000, A snapshot of carbonate reservoir evaluation: Oilfield Review, v. 12, no. 4, p. 20–41.

Alam, M. M., R. Ahsan, A. K. Shaik, and I. L. Fabricius, 2010a, Surface charge of calcite and its influence on the electrical conductivity in chalk (abs.): Society of Exploration Geophysicists Technical Program Expanded Abstracts, v. 29, no. 1, p. 2686–2691, doi:10.1190/1.3513399.

Alam, M. M., M. K. Borre, I. L. Fabricius, K. Hedegaard, B. Røgen, Z. Hossain, and A. S. Krogsbøll, 2010b, Biot's coefficient as an indicator of strength and porosity reduction: Calcareous sediments from Kerguelen Plateau: Journal of Petroleum Science and Engineering, v. 70, no. 3–4, p. 282–297, doi:10.1016/j.petrol.2009.11.021.

Amaefule, J. O., M. Altunbay, D. Tiab, D. G. Kersey, and D. K. Keelan, 1993, Enhanced reservoir description: Using core and log data to identify hydraulic (flow) units and predict permeability in uncored intervals/wells: 68th Society of Petroleum Engineers Annual Technical Conference and Exhibition, Houston, Texas, October 3–6, 1993, SPE Paper 26436, 16 p., doi:10.2523/26436-MS.

Andersen, M. A., 1995, Petroleum research in North Sea chalk: Stavanger, Norway, RF-Rogaland Research, 174 p.

Biot, M. A., 1956a, Theory of propagation of elastic waves in a fluid-saturated porous solid: I. Low-frequency range: The Journal of the Acoustical Society of America, v. 28, p. 168–178, doi:10.1121/1.1908239.

Biot, M. A., 1956b, Theory of propagation of elastic waves in a fluid-saturated porous solid: II. Higher frequency range: The Journal of the Acoustical Society of America, v. 28, p. 179–191, doi:10.1121/1.1908241.

Borre, M., and I. L. Fabricius, 1998, Chemical and mechanical

processes during burial diagenesis of chalk: An interpretation based on specific surface data of deep-sea sediments: Sedimentology, v. 45, no. 4, p. 755–769, doi:10.1046/j.1365-3091.1998.00178.x.

Borre, M. K., and I. L. Fabricius, 2001, Ultrasonic velocities of water-saturated chalk from the Gorm field, Danish North Sea, *in* I. L. Fabricius ed., Sensitivity to stress and applicability of Gassmann's equation: Nordisk Energiforskning, Research in Petroleum Technology, Nordic Petroleum Technology Series V, p. 1–18.

Bramwell, N. P., G. Caillet, L. Meciani, N. Judge, M. Green, and P. Adam, 1999, Chalk exploration: The search for a subtle trap: Geological Society (London) Special Publication 5, p. 911–937.

Britannica Online, 2010, Clay mineral: http://www.britannica.com/EBchecked/topic/120723/clay-mineral (accessed September 14, 2010).

Brunauer, S., P. H. Emmett, and E. Teller, 1938, Adsorption of gases in multimolecular layers: Journal of the American Chemical Society, v. 60, no. 2, p. 309–319, doi:10.1021/ja01269a023.

Carman, P. C., 1937, Fluid flow through granular beds: Chemical Engineering Research and Design, v. 15, p. 150–166.

Darcy, H., 1856, Les fontaines publiques de la ville de Dijon: Paris, Dalmont, 647 p.

D'Heur, M., 1984, Porosity and hydrocarbon distribution in the North Sea chalk reservoirs: Marine and Petroleum Geology, v. 1, p. 211–238, doi:10.1016/0264-8172(84)90147-8.

Du Bernard, X., M. Prasad, and M. Reinstaedtler, 2003, The effect of cementation on the seismic properties of sandstones, *in* W. Arnold and S. Hirsekorn, eds., Acoustical imaging: New York, Kluwer Academic Publishers, v. 27, p. 399–406.

Dunham, R. J., 1962, Classification of carbonate rocks according to depositional texture, *in* W. E. Ham, ed., Classification of carbonate rocks: AAPG Memoir 1, p. 108–121.

Dvorkin, J., and A. Nur, 1996, Elasticity of high-porosity sandstones: Theory for two North Sea data sets: Geophysics, v. 61, no. 5, p. 1363–1370, doi:10.1190/1.1444059.

Fabricius, I. L., 2001, Compaction of microfossil and clay-rich chalk sediments: Physics and Chemistry of the Earth Part A—Solid Earth and Geodesy, v. 26, no. 1–2, p. 59–62, doi:10.1016/S1464-1895(01)00023-0.

Fabricius, I. L., 2003, How burial diagenesis of chalk sediments controls sonic velocity and porosity: AAPG Bulletin, v. 87, no. 11, p. 1755–1778, doi:10.1306/06230301113.

Fabricius, I. L., G. T. Baechle, G. P. Eberli, and R. Weger, 2007a, Estimating permeability of carbonate rocks from porosity and v(p)/v(s): Geophysics, v. 72, no. 5, p. E185–E191, doi:10.1190/1.2756081.

Fabricius, I. L., B. Røgen, and L. Gommesen, 2007b, How depositional texture and diagenesis control petrophysical and elastic properties of samples from five North Sea chalk fields: Petroleum Geoscience, v. 13, no. 1, p. 81–95, doi:10.1144/1354-079306-707.

Fabricius, I. L., L. Gommesen, A. Krogsbøll, and D. Olsen, 2008, Chalk porosity and sonic velocity versus burial depth: Influence of fluid pressure, hydrocarbons, and mineralogy: AAPG Bulletin, v. 92, no. 2, p. 201–223, doi:10.1306/10170707077.

Fabricius, I. L., G. T. Baechle, and G. P. Eberli, 2010, Elastic moduli of dry and water-saturated carbonates: Effect of depositional texture, porosity and permeability: Geophysics, v. 75, no. 3, p. N65–N78, doi:10.1190/1.3374690.

Frykman, P., 2001, Spatial variability in petrophysical properties in upper Maastrichtian chalk outcrops at Stevns Klint, Denmark: Marine and Petroleum Geology, v. 18, no. 10, p. 1041–1062, doi:10.1016/S0264-8172(01)00043-5.

Hamilton, E. L., 1976, Variations of density and porosity with depth in deep-sea sediments: Journal of Sedimentary Research, v. 46, no. 2, p. 280–300.

Han, D., A. Nur, and D. Morgan, 1986, Effects of porosity and clay content on wave velocities in sandstones: Geophysics, v. 51, no. 11, p. 2093–2107, doi:10.1190/1.1442062.

Japsen, P., 1998, Regional velocity-depth anomalies, North Sea chalk: A record of overpressure and Neogene uplift and erosion: AAPG Bulletin, v. 82, no. 11, p. 2031–2074.

Klimentos, T., and C. McCann, 1990, Relationships among compressional wave attenuation, porosity, clay content, and permeability in sandstones: Geophysics, v. 55, no. 8, p. 998–1014, doi:10.1190/1.1442928.

Klinkenberg, L. J., 1941, The permeability of porous media to liquids and gases: Drilling and Production Practice, v. 2, p. 200–213.

Kozeny, J., 1927, Ueber kapillare Leitung des Wassers im Boden: Wien, Sitzungsberichte der Akademie der Wissenschaften, v. 136, p. 271–306.

Kroenke, L. W., et al., 1991, Proceedings of the Ocean Drilling Program, initial reports: College Station, Texas, Ocean Drilling Program, v. 130, 1240 p., doi:10.2973/odp.proc.ir.130.101.1991.

Larsen, I., 1998, Oil and gas production in Denmark: Copenhagen, Denmark, Danish Energy Agency, Ministry of Environment and Energy, v. 98, p. 108.

Madsen, L., and I. Lind, 1998, Adsorption of carboxylic acids on reservoir minerals from organic and aqueous phase: Society of Petroleum Engineers Reservoir Evaluation and Engineering, v. 1, no. 1, p. 47–51.

Mortensen, J., F. Engstrøm, and I. Lind, 1998, The relation among porosity, permeability, and specific surface of chalk from the Gorm field, Danish North Sea: Society of Petroleum Engineering Reservoir Evaluation and Engineering, v. 1, no. 3, p. 245–251, doi:10.2118/31062-PA.

Munns, J. W., 1985, The Valhall field: A geological overview: Marine and Petroleum Geology, v. 2, no. 1, p. 23–43, doi:10.1016/0264-8172(85)90046-7.

Nur, A., G. Mavko, J. Dvorkin, and D. Galmudi, 1998, Critical porosity: A key to relating physical properties to porosity in rocks: The Leading Edge, v. 17, no. 3, p. 357–362, doi:10.1190/1.1437977.

Olsen, C., T. Hongdul, and I. L. Fabricius, 2008, Prediction of Archie's cementation factor from porosity and permeability through specific surface: Geophysics, v. 73, no. 2, p. E81–E87, doi:10.1190/1.2837303.

Pourmohammadi, S., S. Hetland, K. Spildo, and A. Skauge, 2007, Fluid-flow properties of different carbonate pore classes: Society of Petroleum Engineers/European Association of Geoscientists and Engineers Reservoir Characterization and Simulation Conference, Abu Dhabi, United Arab Emirates, October 28–31, 2007, SPE Paper 111433-MS, 11 p., doi:10.2118/111433-MS.

Prasad, M., 2003, Velocity-permeability relations within hydraulic units: Geophysics, v. 68, no. 1, p. 108–117, doi:10.1190/1.1543198.

Prasad, M., and J. Dvorkin, 2001, Velocity to porosity transform in marine sediments: Petrophysics, v. 42, no. 5, p. 429–437.

Raymer, L. L., E. R. Hunt, and J. S. Gardner, 1980, An improved sonic transit time-to-porosity transform: Society of Professional Well Log Analysts, 21st Annual Logging Symposium Transactions, p. 1–13.

Røgen, B., and I. L. Fabricius, 2002, Influence of clay and silica on permeability and capillary entry pressure of chalk reservoirs in the North Sea: Petroleum Geoscience, v. 8, no. 3, p. 287–293, doi:10.1144/petgeo.8.3.287.

Røgen, B., I. L. Fabricius, P. Japsen, C. Høier, G. Mavko, and J. M. Pedersen, 2005, Ultrasonic velocities of North Sea chalk samples: Influence of porosity, fluid content and texture: Geophysical Prospecting, v. 53, no. 4, p. 481–496, doi:10.1111/j.1365-2478.2005.00485.x.

Rogers, S., C. Enachescu, R. Trice, and K. Buer, 2007, Integrating discrete fracture network models and pressure transient data for testing conceptual fracture models of the Valhall chalk reservoir, Norwegian North Sea: Geological Society (London) Special Publication 270, no. 1, p. 193–204, doi:10.1144/GSL.SP.2007.270.01.13.

Schlanger, S. O., and R. G. Douglas, 1974, The pelagic ooze-chalk-limestone transition and its implications for marine stratigraphy, *in* K. J. Hsu and H. C. Jenkyns, eds., Pelagic sediments: On land and under the sea: International Association of Sedimentologists Special Publication 1, p. 117–148.

Scholle, P. A., 1977, Chalk diagenesis and its relation to petroleum exploration: Oil from chalks, a modern miracle?: AAPG Bulletin, v. 61, no. 7, p. 982–1009.

Sverdrup, H. U., M. W. Johnson, and R. H. Fleming, 1942, The oceans, their physics, chemistry, and general biology: New York, Prentice-Hall, 1087 p.

Teeuw, D., 1971, Prediction of formation compaction from laboratory compressibility data: Society of Petroleum Engineers Journal, v. 11, no. 3, p. 263–271, doi:10.2118/2973-PA.

Wyllie, M. R. J., A. R. Gregory, and L. W. Gardner, 1956, Elastic wave velocities in heterogeneous and porous media: Geophysics, v. 21, no. 1, p. 41–70, doi:10.1190/1.1438217.